New insight from noble gas and stable isotopes of geothermal/ hydrothermal fluids at Caviahue-Copahue Volcanic Complex: Boiling steam separation and water-rock interaction at shallow depth

Emilie Roulleau [a,b,*], Daniele Tardani [a,b], Yuji Sano [c], Naoto Takahata [c], Nicolas Vinet [a,b], Francisco Bravo [a], Carlos Muñoz [a], Juan Sanchez [a]

[a] Department of Geology, Universidad de Chile, 8370450 Santiago, Chile
[b] Andean Geothermal Center of Excellence (CEGA), Universidad de Chile, 8370450 Santiago, Chile
[c] The University of Tokyo, Atmosphere and Ocean Research Institute, Kashiwa 277-8564, Japan

ARTICLE INFO

ABSTRACT

We measured noble gas and stable isotopes of the geothermal and hydrothermal fluids of the Caviahue-Copahue Volcanic Complex (CCVC), one of the most important geothermal systems in Argentina/Chile, in order to provide new insights into fluid circulation and origin. With the exception of Anfiteatro and Chancho-co geothermal systems, mantle-derived helium dominates in the CCVC fluids, with measured $^3He/^4He$ ratios up to 7.86Ra in 2015. Their positive $\delta^{15}N$ is an evidence for subducted sediment-derived nitrogen, which is commonly observed in subduction settings. Both He-N_2-Ar composition and positive correlation between δD-H_2O and $\delta^{18}O$-H_2O suggest that the fluids from Anfiteatro and Chancho-co (and partly from Pucon-Mahuida as well, on the southern flank of Copahue volcano) represent a meteoric water composition with a minor magmatic contribution. The Ne, Kr and Xe isotopic compositions are entirely of atmospheric origin, but processes of boiling and steam separation have led to fractionation of their elemental abundances. We modeled the CCVC fluid evolution using Rayleigh distillation curves, considering an initial air saturated geothermal water (ASGW) end-member at 250 and 300 °C, followed by boiling and steam separation at lower temperatures (from 200 °C to 150 °C). Between 2014 and 2015, the CCVC hydrogen and oxygen isotopes shifted from local meteoric water-dominated to andesitic water-dominated signature. This shift is associated with an increase of $\delta^{13}C$ values and S_{total}, HCl and He contents. These characteristics are consistent with a change in the gas ascent pathway between 2014 and 2015, which in turn induced higher magmatic-hydrothermal contribution in the fluid signature. The composition of the magmatic source of the CCVC fluids is: $^3He/^4He = 7.7Ra$, $\delta^{15}N = +6‰$, and $\delta^{13}C = -6.5‰$. Mixing models between air-corrected He and N suggest the involvement of 0.5% to 5% of subducted sediments in the magmatic source. The magmatic sulfur isotopic composition is estimated at $-2.38‰$ (from COP-2), but most samples show elemental fractionation due to boiling and steam separation followed by various degrees of atmospheric contamination. All these geochemical and isotopic characteristics are the direct consequence of tectonic particularities of the CCVC: NE faults promote the ascent of hydrothermal fluids in the geothermal area whereas WNW faults serve as preferential channels for meteoric water infiltration.

1. Introduction

Noble gases have great potential as tracers for mantle sources and fingerprinting of geothermal reservoirs (Sano and Fischer, 2013; Pinti et al., 2013). The noble gases present in hydrothermal fluids are from three potential sources: the crust, the mantle, and the atmosphere. Hydrothermal fluids are characterized by freshwater that contains atmospheric noble gases dissolved during recharge. This water in a geothermal reservoir is responsible for continuous energy and mass transfer from depth to the surface. Over time, this water geochemically evolves due to addition of radiogenic isotopes (^4He and ^{40}Ar) during continuous high-temperature water-rock interactions (Kennedy and van Soest, 2006). Most importantly, the He isotopic composition differs by three orders of magnitude between crust and mantle. Thus, this value has the potential to distinguish He mantle-derived fluids that provide the heat energy from the magmatic activity into the system (Sano and Fischer, 2013; Hilton et al., 2002). The implication of the three above-mentioned components in the geothermal system is essential to understand the origin of the thermal fluids, their pathway and subsurface interaction. Noble gases have a low solubility in freshwater, particularly at

* Corresponding author at: Universidad de Chile, Departmento de Geology and Andean Geothermal Centre of Excellence (CEGA), Plaza Ercilla 803, Santiago, Chile.
E-mail addresses: eroulleau@ing.uchile.cl, roulleau_emilie@yahoo.fr (E. Roulleau).

high temperature (Crovetto et al., 1982). Phase separation during boiling in the geothermal system can generate a residual liquid that becomes depleted in noble gases and isotopically fractionated compared to the initial fluid composition. Thus, noble gases are useful to discriminate the magmatic origin, constrain active geothermal areas of interest, and determine physical processes related to magmatic degassing or hydrothermal circulation. To date, systematic studies using noble gases in a single volcanic system/geothermal reservoir in Chile are not available. Therefore, we performed a study of noble gases along with stable isotopes at the Caviahue-Copahue Volcanic Complex (CCVC) where magma emplacement and fluid flow are strongly controlled by the northern termination of the Liquiñe-Ofqui Fault Zone (LOFZ) associated with a second-order anisotropy of overall NE-SW and NW-SE orientation. This geothermal/hydrothermal system of CCVC has been investigated for various purposes; geothermic energy and volcanic risk. However, some lacks still exist about the processes of boiling and steam separation and the location of the water recharge area. Previous study from Agusto et al. (2013) suggests the presence of preferential water recharge of the geothermal system in Chancho-co and Anfiteatro areas, additionally with the water recharge coming from the flank of the Copahue volcano. Agusto and Varekamp (2015) indicated that the evaporation process occurs in the geothermal system at the same temperature (30 °C) that as the Copahue crater lake (30 °C represents the low-end range temperature of the crater lake). Knowing that the geothermal reservoir has a temperature of 250 °C–300 °C (Agusto et al., 2013) and that the temperature of fumaroles and bubbling gas is around the boiling temperature, it is difficult to confirm an evaporation process at 30 °C.

Thus, in the present study, we present new chemical and isotopic composition ($\delta^{15}N$, $\delta^{13}C$-CO_2, $\delta^{13}C$-CH_4, $\delta^{34}S$, $^3He/^4He$, δD-H_2O, and $\delta^{18}O$-H_2O) of fumaroles, bubbling gases from thermal springs, and one well surrounding the CCVC, all collected in 2014 and 2015, that explore the possibility that Chancho-co and Anfiteatro represent preferential areas of fluid-rock-groundwater interaction without any implication for water recharge of the geothermal system. We also suggest that the boiling steam separation is effective between 190 °C and 150 °C that corresponds more or less at the temperature of the vapor-dominated zone (180 °C–200 °C; Agusto et al., 2013). Thus, the aim of this work is to couple noble gases with other water tracers in order to: 1) better identify water-rock-fluid interactions at shallow depth, 2) determine how boiling and steam separation affect the elemental and isotopic fractionation, 3) identify the deep magmatic source, and 4) establish a relationship between the geochemical composition of the geothermal fluids and the fault network.

2. Geology

In the Southern Volcanic Zone (SVZ) of Chile and Argentina, geothermal activity occurs in close spatial relationship with active volcanism along the Cordillera which is primarily controlled by the ~1000 km long, NNE-trending Liquiñe-Ofqui Fault Zone (LOFZ), an intra-arc dextral strike-slip fault system associated with second-order anisotropy of overall NE-SW (extensional) and NW-SE (compressional) orientation (Fig. 1) (Cembrano et al., 1992, 1996, 2000; Cembrano and Lara, 2009).

The Caviahue-Copahue Volcanic Complex (CCVC) is located at 37.5°S, 71°W, at the border between Argentina and Chile (Fig. 1), and is composed of the Caviahue caldera and the Copahue stratovolcano (Fig. 1). Structurally, the CCVC is located in the accommodation zone at the northern termination of the LOFZ (Melnick et al., 2006). The Caviahue caldera is a square-shaped depression of ca. 20 km × 15 km, defined as a transitional pull-apart, intra-arc basin due to the local stress field generated by the interaction of the LOFZ and the Antiñir Copahue
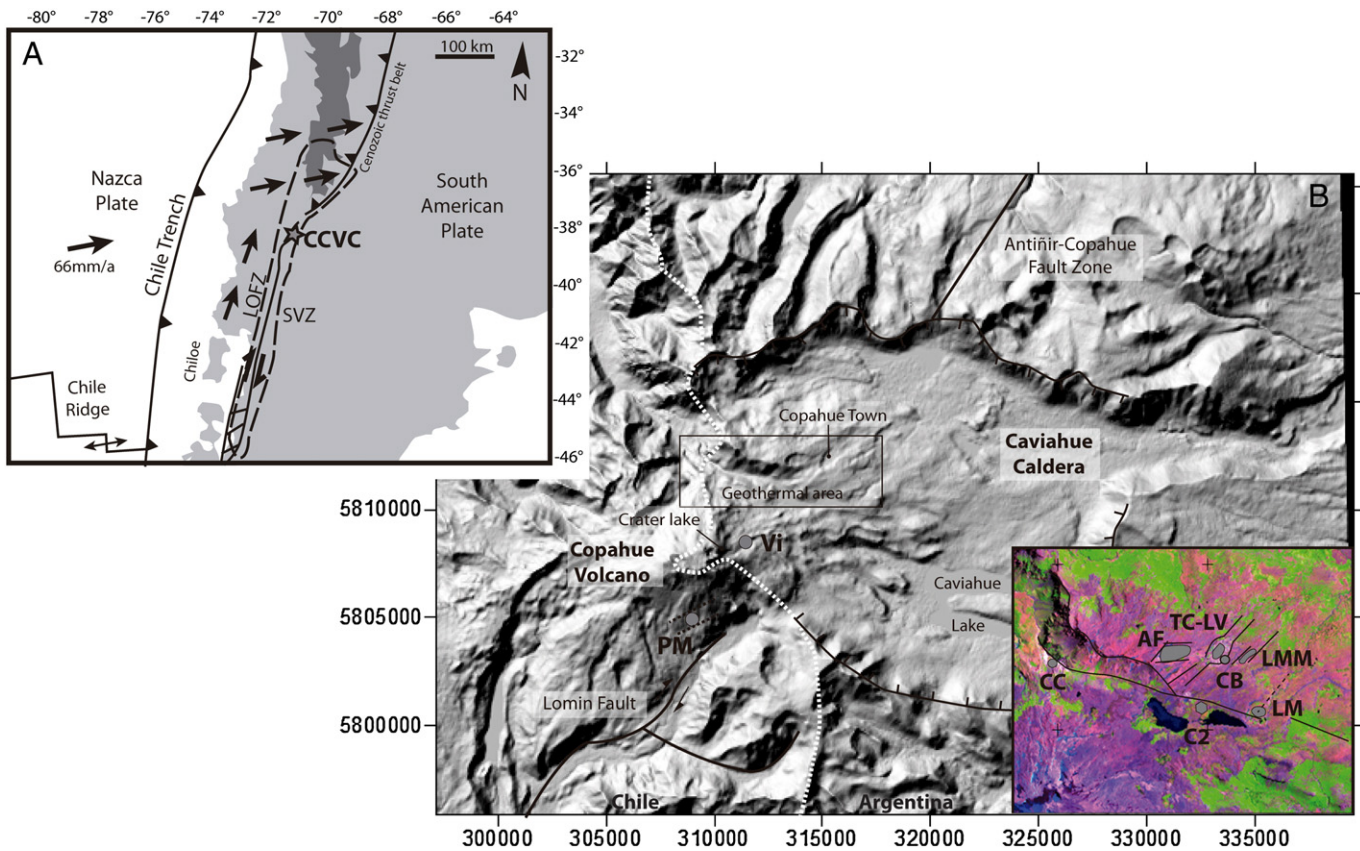

Fig. 1. A) Simplified map of South America with location of the Copahue-Caviahue Volcanic Complex (CCVC; Melnick et al., 2006). LOFZ, Liquiñe-Ofqui Fault Zone; SVZ, South Volcanic Zone. B) Simplified structural map of the Caviahue caldera. This map reports the main structures and active geothermal/hydrothermal areas: Las Maquinas (LM), Las Maquinitas (LMM), Anfiteatro (AF), Termas Copahue (TC-LV), Cabañita (CB), Chancho-co (CC), Pucon Mahuida (PM), Vertientes (Vi) and C2 (COP-2). Grey circles are for fumarole and bubbling pool samples; grey diamond is for the deep well sample.

fault zone (ACFZ). The ACFZ is a thrust system that begins at the latitude of the Caviahue caldera and is responsible for its development.

The history of the Caviahue caldera started at 3–4 Ma with the opening of a pull-apart caldera. The walls and basement of the Caviahue caldera are defined by the Cola de Zorro Formation (5–6 Ma; Linares et al., 1999), which is composed of basaltic and andesitic lavas, volcanic breccias and minor sedimentary beds continuously exposed in the main Cordillera between 36° and 39°S. Las Mellizas volcano formed inside the caldera is composed of three sequences: lower lavas, ignimbrites, and upper lavas. The ignimbrites represent the collapse of Las Mellizas stratovolcano (Melnick et al., 2006) dated by K/Ar at 3.2 ± 0.14 Ma and 2.6 ± 0.1 Ma (Linares et al., 1999). The Copahue volcano is an active andesitic to basaltic–andesitic stratovolcano nested on the western rim of the Caviahue caldera. Volcanic activity at Copahue began at approximately 1 Ma ago. However, since the Upper Pleistocene and postglacial period, activity has consisted mainly in effusive emissions of andesitic lava flows and only a few explosive episodes during the Holocene that generated at least 6 ash flows (Linares et al., 1999; Muñoz and Stern, 1988). During the last 250 years, the Copahue eruptions have consisted in weak phreatic and phreatomagmatic events. Since Nov.–Dec. 2011, the discharge of fluids from the summit of Copahue volcano has significantly increased and intermittent phreatic events occurred since 2012, with a big eruption reported in Dec. 2012 (Caselli et al., 2015). Copahue volcano holds an acidic crater lake (Temp.: 8 °C–19 °C ; pH ~ 0.2–1.1; Varekamp et al., 2009; Agusto and Varekamp, 2015: Fig. 1) and acidic hot springs called Vertientes (Vi; Temp. : 40 °C–70 °C ; pH ~ 0.3–2.4; Fig. 1) near the summit area; all feed the Agrio river (pH ~ 0.5–2.5). This river discharges into a large glacial lake, called Lake Caviahue, and acidified it (pH: 2.1–2.7; Agusto, 2011; Caselli et al., 2005; Varekamp et al., 2001., 2009).

Five geothermal areas are recognized in the region, with surface manifestations including boiling pools and bubbling pools with temperatures reaching up to 96 °C, and fumaroles that reach temperatures of up to 135 °C (Agusto et al., 2007). The Las Maquinas (LM), Las Maquinitas (LMM), Termas de Copahue (TC-LV), Cabanita (CB) and Anfiteatro (AF) thermal areas are located northeast of the volcano and appear to be controlled by the northeast structures (Melnick et al., 2006). The Chancho-co (CC) geothermal field is located on the northern flank of the volcano, in close proximity to the volcanic–hydrothermal system (Velez et al., 2011). The Pucon-Mahuida (PM) bubbling gas manifestation lies in the southern flank of Copahue volcano and represents a direct manifestation of the hydrothermal system from Copahue volcano (Fig. 1). The geothermal field of CCVC had been defined as a vapor-dominated field with stratified layers connected by fractures with increased vertical permeability within the reservoir (Agusto et al., 2013; Panarello, 2002; JICA, 1992). During geothermal exploration of the CCVC, a vapor-dominated hydrothermal system was recognized in its northeastern part, composed of two different productive reservoirs located at depths of 800–1000 m and 1400 m, with temperatures estimated from geothermometry at 180–200 °C and 250–300 °C, respectively (Agusto et al., 2013), whereas the basis of temperature from drilling
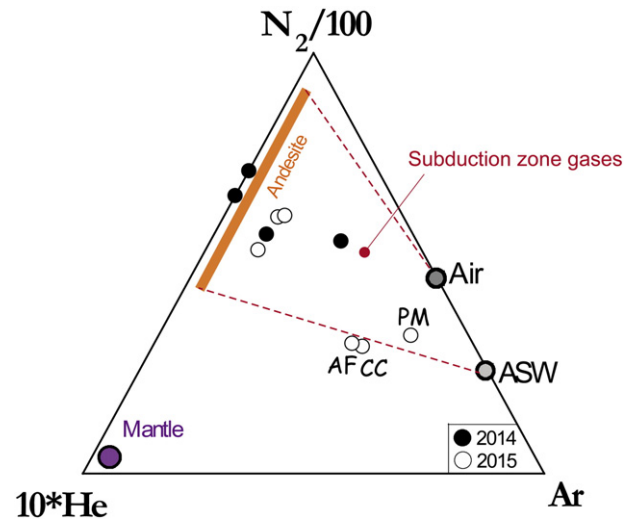

Fig. 2. He-N_2-Ar ternary diagram (Giggenbach and Poreda, 1993) presenting the chemical composition of the CCVC fluids. The He-N_2-Ar composition of our samples is typical of subduction-zone gases. Most samples are close to the andesite field, with the exception of PM, CC and AF that show strong interaction with the Air-Saturated Water (ASW) end-member. Chanco-co sample from 2014 was not plotted because Ar was not detected.

ranges from 235 °C (COP-2 and COP-4) to 250 °C (COP-1; Mas and Mas, 2015). According to the measurements carried out in the wells drilled up to now, the reservoir parameters were defined by a static pressure up to 4 MPa and a flow rate up to 50–60 t/h (Mas, 2005).

3. Sampling and methods

During 2014 and 2015, we collected twenty gas samples, more duplicate, from fumaroles, bubbling gases, one water and one well (COP-2), all from the CCVC geothermal areas. Fumarole gases were sampled using a titanium tube connected by a silicone tube to an alkaline glass bottle and a cold trap. The alkaline glass bottle and cold trap were plunged in cold water. Bubbling gas samples were collected using an alkaline glass container with vacuum valves at both ends, following a water displacement method. Gas samples from fumarole and bubbling gas emanation were also collected into Pyrex flasks (Giggenbach bottles) containing 20 mL of 4 N NaOH solution for absorption of acid gas for gas composition analyses. One water sample from the natural hot spring from Chancho-co was collected in alkaline glass containers using a manual pump.

Noble gases were analyzed at the Noble Gas Laboratory of the University of Michigan, USA. Gas samples were attached to a vacuum extraction system and noble gases were quantitatively extracted for inletting into a MAP-215 mass spectrometer for isotopic analyses. Extracted gases were passed over a Ti sponge getter to remove reactive

Table 1
Chemical composition of the dry gas fraction (in ppm) and water vapor (in %) of the CCVC gases.

Location of analyzes	Sample	Location	Type	Date	CO_2	S_{total}	N_2	CH_4	H_2	HCl	HF	Ar	O_2	He	H_2O
Taiwan	COP-LMM-FI-14	Las Maquinitas (LMM)	Fumarole	2014	944354	10187	18813	10930	15485	203	n.d.	n.d.	n.d.	9.64	97.58
Taiwan	COP-LM-FI-14	Las Maquinas (LM)	Fumarole	2014	941690	7390	15450	17380	17804	261	n.d.	n.d.	n.d.	6.02	97.53
Taiwan	COP-CC-FI-14	Chanco-co (CC)	Fumarole	2014	884104	86140	995	740	27342	663	n.d.	n.d.	n.d.	1.36	99.25
Taiwan	COP-LMM-BG-14	Las Maquinitas (LMM)	Bubbling gas	2014	921650	12110	28397	15385	22044	313	n.d.	56.81	n.d.	15.82	95.15
Taiwan	COP-CB-FI-14	Cabanita (CB)	Fumarole	2014	941371	17378	28856	10045	2006	172	n.d.	147.51	n.d.	8.56	96.77
USA	COP-2-GW-15	COP-2 (C2)	Well	2015	922573	18342	29477	17484	11366	491	n.d.	63	185	19.59	95.04
USA	COP-AF-FI-15	Anfiteatro (AF)	Fumarole	2015	826200	59069	54300	44408	14553	n.d.	592	815	19.6	43.61	98.78
USA	COP-PM-BG-15	Pucon Mahuida (PM)	Bubbling gas	2015	970450	18523	8760	201	n.d.	268	66	146	1583	3.32	–
USA	COP-LM-FI-15	Las Maquinas (LM)	Fumarole	2015	905588	27735	31479	20653	13551	647	229	61	43.87	14.02	97.06
USA	COP-CC-FI-15	Chanco-co (CC)	Fumarole	2015	652434	261853	19715	3823	50557	6249	4606	273	473	16.66	99.68
USA	COP-CB-FI-15	Cabanita (CB)	Fumarole	2015	912957	32895	28981	14887	9163	792	242	62	8.4	12.03	97.52

Note: S_{total} is mainly composed of H_2S. n.d.: not detected.

Table 2
Isotopic composition of the CCVC fluids.

Samples	Field zone	Type	Longitude –E (19H; WSG84)	Latitude -S (19H; WSG84)	T (°C)	$\delta^{15}N$ ‰	+/−	$\delta^{13}C$–CO_2 ‰	+/−	$\delta^{13}C$–CH_4 ‰	+/−	$\delta^{34}S$ ‰	+/−
COP-LM-FI-14	Las Maquinas (LM)	Fumarole	316576	5810568	93.1	4.93 [a]	0.20	−7.96 [a]	0.14	−34.38	0.14	n.a.	
COP-CB-FI-14	Cabanita (CB)	Fumarole	315424	5812052	93.1	n.a.		−8.10	0.14	−30.77	0.14	n.a.	
COP-LMM-BG-14	Las Maquinitas (LMM)	Bubbling gas	316316	5812178	93.2			−7.38	0.14	n.a.		n.a.	
COP-CC-FI-14	Chancho-co (CC)	Fumarole	309674	5812036	94.8	−0.86	0.20	−9.82	0.14	n.a.		1.37	0.23
COP-AF-FI-14	Anfiteatro (AF)	Fumarole	313709	5812304	93	2.11	0.20	−7.90	0.14	−45.99	0.14	n.a.	
COP-PM-BG-14	Pucon Mahuida (PM)	Bubbling gas	308709	5803399	42	4.42 [a]	0.21	−11.87 [a]	0.14	n.a.		n.a.	
COP-CB-FI -15	Cabanita (CB)	Fumarole	315405	5812012	92	n.a.		n.a.		n.a.		n.a.	
COP-AF-FI-15	Anfiteatro (AF)	Fumarole	313894	5812237	92.3	1.77	0.22	−6.52	0.28	−37.51	0.27	-2.77	0.14
COP-AF-BG-15	Anfiteatro (AF)	Bubbling gas	313885	5812227	86	0.15	0.22	−6.18	0.30	−30.81	0.28	n.a.	
COP-CC2-FI-15	Chancho-co (CC)	Fumarole	309609	5812050	95.2	n.a.		−6.92	0.27	n.a.		n.a.	
COP-CC3-W-15	Chancho-co (CC)	Water	310389	5811855	73.6	−1.46	0.22	−8.24	0.27	−36.36	0.30	n.a.	
COP-2-WG-15	COP-2 (C2)	Well	314718	5810935	220	3.59	0.23	−6.96	0.27	−18.23	0.27	-2.38	0.31
COP-LM-FI-15	Las Maquinas (LM)	Fumarole	316598	5810512	93	4.11	0.22	−6.95	0.27	−28.07	0.27	-4.21	0.40
COP-LM-BG-15	Las Maquinas (LM)	Bubbling gas	316399	5810236	92.5	3.61	0.22	−6.52	0.28	−30.16	0.27	2.56	0.13
COP-LM2-BG-15	Las Maquinas (LM)	Bubbling gas	316895	5810524	92.5	3.27	0.22	−6.27	0.29	−25.65	0.27	1.68	0.20
COP-LMM-BG-15	Las Maquinitas (LMM)	Bubbling gas	316322	5812176	94.5	1.95	0.22	−6.02	0.28	−26.56	0.27	n.d.	
COP-LV-BG-15	Termas Copahue (LV)	Bubbling gas	315415	5812305	35.2	2.33	0.22	−6.11	0.27	−24.53	0.27	-4.86	0.62
COP-TC-BG-15	Termas Copahue (TC)	Bubbling gas	315212	5812251	92	n.a.		−6.45	0.28	−26.02	0.27	n.a.	
COP-PM-BG-15	Pucon Mahuida (PM)	Bubbling gas	308509	5803096	42	4.02	0.24	−10.45	0.27	n.a.		n.a.	

Note: n.a.: not analyzed. *: Gas composition was determined by comparing peak heights of the samples with those of standard gases, using a quadrupole mass spectrometer at AORI-The University of Tokyo. Experimental errors were estimated to be about ± 10% by repeated measurements of standard samples. The measured blank for each component was negligibly small compared to the sample signal. The $CO_2/^3He$ and $CH_4/^3He$ ratios were calculated using $^3He/^4He$ and CO_2/He, and CH_4/He, respectively. (a) Data from Tardani et al. (2016). (b) Percentage of sediment-derived nitrogen in binary sediment-mantle mixture. (c) Measured nitrogen isotope ratios are corrected for air contamination using $\delta^{15}N_C = f \times \delta^{15}N_{MORB} + (1 - f) \delta^{15}N_{Sed}$, where $\delta^{15}N_{MORB} = -5‰$, $\delta^{15}N_{Sed} = +7‰$, and f is the fraction of mantle-derived nitrogen [calculated from: f = 1 - (%Sed./100)]. The $\delta^{15}N_C$ values were not estimated for Chancho-co and Anfiteatro that are affected by meteoric water interaction.

gases, and sequentially allowed to enter the MAP-215 mass spectrometer using a cryo-separator. The ^4He, ^{20}Ne, and ^{40}Ar were measured using a Faraday detector while all other isotopes were measured using an electron multiplier in ion counting mode. During neon isotope analysis, a liquid N_2 cold trap was applied to minimize peak interferences. The interference corrections for ^{20}Ne and ^{22}Ne were typically 1.1% and 0.17%, respectively. Isotopic abundances for each sample were normalized to the air standard after blank correction. Elemental abundances of ^4He, ^{22}Ne, ^{36}Ar, ^{84}Kr, and ^{132}Xe have typical uncertainties of 1.5%, 1.3%, 1.3%, 1.5%, and 2.2%, respectively, and all uncertainties are at ± 1σ level.

The $^3He/^4He$ ratio was measured on a conventional noble gas mass spectrometer (Helix-SFT) at AORI-The University of Tokyo, Japan. The $^4He/^{20}Ne$ ratio was measured using an online quadrupole mass spectrometer. Helium was separated from Ne using a cryogenic trap held at 40 K (Sano and Wakita, 1988). The observed $^3He/^4He$ ratio was calibrated against atmospheric helium. Experimental errors for $^4He/^{20}Ne$ and $^3He/^4He$ ratios with the Helix spectrometer were about 5% and 1%, respectively at 1σ (Sano et al., 2008).

The $^3He/^4He$ ratio was corrected for the presence of atmospheric He, using the He/Ne ratio of the sample (Craig et al., 1978). It is assumed that Ne in magmatic and crustal gases is negligible, and that essentially all Ne in geothermal gas samples is atmospheric (see equation details in Sano et al., 2006). The air-corrected $^3He/^4He$ ratio is denoted Rc/Ra. The error assigned to the corrected $^3He/^4He$ ratio in Table 1 defined the $^3He/^4He$ propagated errors (Sano et al., 2006).

Argon isotopic analyses were also performed at AORI-The University of Tokyo. The $^{40}Ar/^{36}Ar$ ratios were measured using an online quadrupole mass spectrometer (Massmate100, ULVAC Co.), after purification using a hot Ti-getter. The measurement error was 1–2% at 1σ.

Nitrogen, sulfur, and carbon (from CO_2 and CH_4) isotopic compositions were determined using an IsoPrime stable isotope ratio mass spectrometer at AORI-The University of Tokyo.

The δ–notation of the isotopic values is conventionally represented with respect to standard and given by equation:

$$\delta X = \left(\left[^{ii}X / ^{i}X \right]_{sample} / \left[^{ii}X / ^{i}X \right]_{std.} - 1 \right) \times 1000 \qquad (1)$$

Measurement errors of $\delta^{15}N$, $\delta^{34}S$, $\delta^{13}C$-CO_2 and $\delta^{13}C$-CH_4 are less than ± 0.2‰, ± 0.3‰, ± 0.2‰ and ± 0.3‰, respectively. It is relevant to note that the $\delta^{34}S$ values refer to the composition of total sulfur that is mainly composed of H_2S.

Oxygen and hydrogen isotopic compositions were determined using an ISOprime stable isotope ratio mass spectrometer at GEOTOP-UQAM (Canada). Measurement uncertainty for ^{18}O and ^2H is ± 0.05‰ (1 s) and ± 1‰ (1 s), respectively.

Gas compositions in fluids were determined at the University of New Mexico, USA, for samples collected in 2015. Inert gases (N_2, O_2, H_2, He, Ar, and CO) were analyzed on a Pfeiffer Quadrupole Mass Spectrometer (QMS). Calibration of the QMS was performed with standard gas mixtures (Scott Specialty Gases; de Moor et al., 2013a). The QMS analyses have a precision of <0.1% (concentration). Carbon dioxide concentrations were determined by titration of NaOH solutions using 0.1 N HCl. Total S was determined gravimetrically after precipitation of $BaSO_4$ from the NaOH solutions, and SO_2/H_2S was measured by alkaline iodine titration (Giggenbach and Goguel, 1989).

For samples collected in 2014, gas compositions were determined at the National Taipei University, Taiwan. Inert gases were analyzed by a gas chromatograph (GC, SRI 8610C). HCl and total sulfur were analyzed with an ion chromatograph (IC, Metrohm 790 Personal). The titration method was applied to measure the CO_2 concentration, (Metrohm 702 SM Titrion) by assuming that all of the CO_2 inside the sample had been dissolved as CO_3^{2-} in the alkali solution (Giggenbach, 1975). SO_2/H_2S proportion was measured by alkaline iodine titration (Lee et al., 2005).

4. Results

4.1. Chemical composition of the CCVC fluids

We report in Table 1 the chemical composition of the dry gas fraction and the molar percentage of water vapor for the CCVC fluids, sampled in 2014 and 2015. The water vapor proportion in fumaroles, bubbling gases and a geothermal well from the CCVC is higher than 95%. The dry gas phase from the CCVC fluids is dominated by CO_2, with around 920,000 ppm for Las Maquinas (LM), Las Maquinitas (LMM), Cabañita (CB), COP-2 (C2), and Pucon-Mahuida (PM), whereas it is lower in

δD-H₂O	δ¹⁸O-H₂O	⁴He/²⁰Ne	R/Ra +/-	Rc/Ra +/-	⁴⁰Ar/³⁶Ar +/-	N₂/Ar	CO₂/³He	CH₄/³He	N₂/He	Carbon contribution			Nitrogen	Contribution
‰	‰						x10⁹	x10⁸		Lim.	MORB	Org.Sed.	%Sed. [b]	δ¹⁵N$_c$ (‰) [c]
-88.4	-10.83	67.55	7.48 0.15 [a]	7.52 0.02	320.7 4.8	545	14.92	2.75	2564	0.71	0.04	0.25	0.95	6.4
-101.2	-14.23	8.51	7.27 0.15	7.51 0.30	289.0 4.2	139	10.80	1.15	3369	–	–	–	–	–
-85.2	-10.65	81.59	7.57 0.15	7.59 0.01	301.7 4.5	213	5.50	0.92	1795	–	–	–	–	–
-105.2	-14.64	3.21	4.78 0.10	5.19 0.45	287.5 4.2	96	96.97	0.81	730	0.67	0.0025	0.3275	–	–
-109.3	-18.25	55.23	5.27 0.11	5.29 0.01	299.8 4.4	116 *	17.10 *	5.15 *	5865 *	0.67	0.085	0.245	–	–
n.a.	n.a.	27.58	6.16 0.12 [a]	6.23 0.02	297.2 4.5	90 *	71.20 *	0.04 *	3362 *	0.59	0.02	0.39	0.95	6.4
n.a.	n.a.	652.17	7.86 0.07	7.86 0.07	371.2 0.8	467	6.90	1.12	2409	–	–	–	–	–
-89.6	-12.11	70.94	5.37 0.03	5.39 0.03	302.2 0.1	67	2.52	1.35	1245	0.74	0.055	0.205	–	–
n.a.	n.a.	0.99	3.76 0.08	4.66 0.08	290.8 8.7	n.a.	–	–	–	–	–	–	–	–
n.a.	n.a.	0.95	3.65 0.02	4.57 0.03	295.4 0.1	72	7.66	0.45	1184	–	–	–	–	–
n.a.	n.a.	1.64	3.70 0.08	4.18 0.08	299.9 9.0	n.a.	n.a.	n.a.	n.a.	–	–	–	–	–
n.a.	n.a.	233.61	7.50 0.06	7.51 0.06	316.5 0.8	467	4.48	0.85	1505	0.565	0.255	0.18	0.88	5.6
-48.0	0.92	562.38	7.09 0.04	7.10 0.04	391.6 6.5	516	6.50	1.48	2245	0.59	0.23	0.18	0.92	6.0
n.a.	n.a.	82.12	7.47 0.15	7.49 0.15	302.3 9.1	315 *	10.84 *	3.38 *	3409 *	0.67	0.145	0.185	0.92	6.0
n.a.	n.a.	-	-	-	297.7 8.9	286 *	–	–	2061 *	0.6	0.245	0.155	0.88	5.6
-47.8	-0.73	12.32	7.32 0.06	7.45 0.06	298.1 0.1	119 *	4.67 *	1.27 *	3822 *	0.56	0.305	0.135	0.88	5.6
n.a.	n.a.	32.43	7.49 0.03	7.55 0.03	297.7 8.9	148 *	6.73 *	1.26 *	3679 *	0.61	0.23	0.16	0.90	5.8
n.a.	n.a.	16.92	7.49 0.09	7.59 0.09	300.0 0.1	116 *	6.20 *	0.95 *	6672 *	0.58	0.26	0.16	0.73	3.8
-84.6	-11.97	14.59	6.49 0.04	6.59 0.04	299.1 0.1	60	27.85	0.07	2637	0.6	0.06	0.34	0.92	6.0

fluids from Chancho-co (CC) and Anfiteatro (AF) (652,434 ppm to 826,200 ppm). Relatively high concentrations of total S (mainly H_2S; from 7390 to 26,1853 ppm), N_2 (from 995 to 54,300 ppm) and CH_4 (from 201 to 44,408 ppm) are observed. The acidic gas species HCl and HF are detected in some samples, ranging from 172 to 6249 ppm and from 66 to 4606 ppm, respectively. The Ar and He concentration is up to 814 ppm and 43 ppm, respectively. In a He-Ar-N ternary diagram (Fig. 2), the CCVC fluids are defined as having an andesitic composition similar to that of subduction zone gases. However, three samples (namely, PM, AF and CC) also present a combination of Air-Saturated Water (ASW) and/or an air component.

4.2. Isotopic composition of gases (δ¹⁵N, δ¹³C-CO₂, δ¹³C-CH₄, δ³⁴S) and water vapor (δD-H₂O, δ¹⁸O-H₂O)

The values of δD-H_2O and δ¹⁸O-H_2O in condensate samples vary over time (Table 2). In 2014 and 2015, δD-H_2O ranged from −109.3‰ to −85.5‰ and from −89.6‰ to −47.8‰, respectively, whereas δ¹⁸O-H_2O varied between −18.25‰ and −10.65‰ in 2014, and between −12.11‰ and 0.92‰, in 2015.

The δ¹⁵N values of all CCVC fluids ranged from 0.77‰ to 4.93‰ (Table 2).

The δ¹³C-CO_2 values for fumaroles and bubbling gases in 2014 ranged from −7.38‰ to −9.82‰, but varied from −6.02‰ to −6.92‰ in 2015 (Table 2). The only water sample from Chancho-co (CC; collected in 2015) had a δ¹³C-CO_2 value of −8.24‰. With δ¹³C-CO_2 of −11.87‰ in 2014 and −10.42‰ in 2015, the samples from Pucon-Mahuida (PM) show a significantly lower value than that of all the geothermal areas.

The δ¹³C-CH_4 of all CCVC fluids excluding Chancho-co (CC) and Anfiteatro (AF) ranged from −34.38‰ to −30.77‰ in 2014 and from −30.16‰ to −18.23‰ in 2015 (Table 2). The δ¹³C-CH_4 value from AF was −45.99‰ in 2014 and ranges from −37.51‰ to −30.81‰ in 2015. The δ¹³C-CH_4 value from CC was −36.36‰ in 2015.

The δ³⁴S values from CCVC fluids show a large variation, from −4.86‰ to 2.56‰.

4.3. Noble gas isotopes

The ³He/⁴He ratios (R/Ra) of Las Maquinas (LM), Las Maquinitas (LMM), Termas Copahue (TC-LV), and Cabañita (CB) samples varied between 7.09Ra and 7.86Ra (Table 2). Values for Chancho-co (CC) and

Anfiteatro (AF) ranged from 3.65Ra to 5.37Ra, and from 6.16Ra to 6.49Ra for Pucon-Mahuida (PM). Fig. 3 illustrates the variation of R/Ra in the CCVC fluids against the ⁴He/²⁰Ne ratios. The regression curves suggest that the He isotopic composition of the CCVC fluids results from a mixing between air (ASW; 1Ra) and a mantle component estimated at 7.7Ra. The samples from Pucon-Mahuida, Chancho-co and Anfiteatro represent a mixing between ASW (1Ra) and values of 6.4Ra and 5.3Ra, respectively, suggesting addition of radiogenic ⁴He in the hydrothermal system from shallow environment (meteoric water and/or local sediments).

The ²⁰Ne/²²Ne and ²¹Ne/²²Ne isotopic ratios of the CCVC fluids ranged from 9.54 to 10.22 and from 0.0269 to 0.0292, respectively (Appendix A). The ¹²⁹Xe/¹³⁰Xe and ¹³⁶Xe/¹³⁰Xe isotopic ratios also

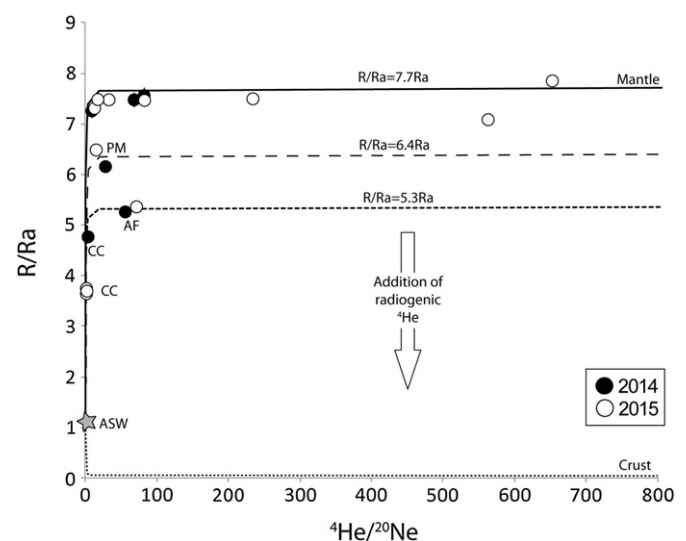**Fig. 3.** ³He/⁴He (R) normalized to the atmospheric ratio (Ra) versus ⁴He/²⁰Ne. Our data are interpreted as a mixing between an atmospheric (ASW) and a mantle component. The CCVC samples with high R/Ra are compatible with a mantle source at 7.7Ra. The 6.4Ra and 5.3Ra curves model well the PM (Pucon-Mahuida), AF (Anfiteatro), and CC (Chancho-co) samples. These samples are affected by progressive dilution through addition of radiogenic He. The 1σ error is smaller than the symbol size.

showed low variation, from 6.294 to 6.523 and from 2.171 to 2.180, respectively (Appendix A). These values are totally similar to the atmospheric component (9.80, 0.0290, 6.496 and 2.176, respectively; Ozima and Podosek, 2002), but they might account for a slight mass fractionation by gaseous diffusion too (Marty, 1984). The $^{38}Ar/^{36}Ar$ isotopic ratios were also atmospheric (0.188; Appendix A). In contrast, the $^{40}Ar/^{36}Ar$ ratios (287.5 to 371.2; Table 2) were similar or higher than that of the atmosphere component (295.5; Ozima and Podosek, 2002), suggesting that they reflect the source of the CCVC fluids.

5. Discussion

5.1. Boiling-steam separation and meteoric water recharge: evidence of elemental fractionation of noble gases

Neon and xenon isotopes have great potential as tracers for mantle sources and fingerprinting of geothermal reservoirs. $^{20}Ne/^{22}Ne$ and $^{21}Ne/^{22}Ne$ ratios are high in MORB (12.6 and 0.060, respectively) compared to air (9.8 and 0.029, respectively; Moreira and Kurz, 2013), while hydrothermal fluids from different settings are characterized by significant air contribution or highly fractionation-related $^{20}Ne/^{21}Ne$ values. In Iceland and Yellowstone (USA), Ne isotopes show mixing between a MORB-type mantle and air components (Sano and Fischer, 2013, and authors therein). However, in subduction settings, $^{20}Ne/^{22}Ne$ and $^{21}Ne/^{22}Ne$ ratios suggest a significant crustal contribution (Tedesco et al., 1998), with the exception of Etna volcano that has extremely high $^{20}Ne/^{22}Ne$ and $^{21}Ne/^{22}Ne$ ratios, close to the MORB field (Nakai et al., 1997). Xenon has many isotopes but the most representative ratios are $^{129}Xe/^{130}Xe$ and $^{136}Xe/^{130}Xe$. The MORB $^{129}Xe/^{130}Xe$ and $^{136}Xe/^{130}Xe$ ratios lie at 7.7 (Moreira and Kurz, 2013) and 2.6 (Trieloff et al., 2000), respectively. In subduction settings, xenon from hydrothermal fluids mainly originates from the atmosphere ($^{129}Xe/^{130}Xe = 6.49$ and $^{136}Xe/^{130}Xe = 2.16$; Pinti et al., 2013).

The Ne and Xe (and Kr) isotopic ratios of the CCVC fluids are close to atmospheric values (Appendix A) and show a slight mass fractionation by gaseous diffusion (Marty, 1984). These two observations represent typical isotopic characteristics in arc setting but cannot help the better understanding of the CCVC fluid features because the original Ne, Xe and Kr isotopic compositions are masked by these two processes.

Noble gas relative abundances (Table 3) are given using the F-value notation (Ozima and Podosek, 2002) in which measured abundances are normalized to the air abundance with ^{36}Ar as the reference isotope [e.g., $F(i) = (i / ^{36}Ar)_{sample} / (i / ^{36}Ar)_{air}$]. Pinti et al. (2013) presented $F(^{132}Xe)$, $F(^{20}Ne)$ and $F(^{84}Kr)$ data from Los Azufres (Mexico) and showed that elemental abundances can be useful fingerprints of physical changes in the reservoir caused by boiling and steam separation and meteoric water interaction, and are easily fractionated compared to the equilibrium solubility concentrations (Mazor and Truesdell, 1984). Fig. 4A shows $F(^{132}Xe)$ versus R/Ra values measured in the CCVC fluids in 2014 (black circle) and 2015 (empty circle). R/Ra and F(i) values for
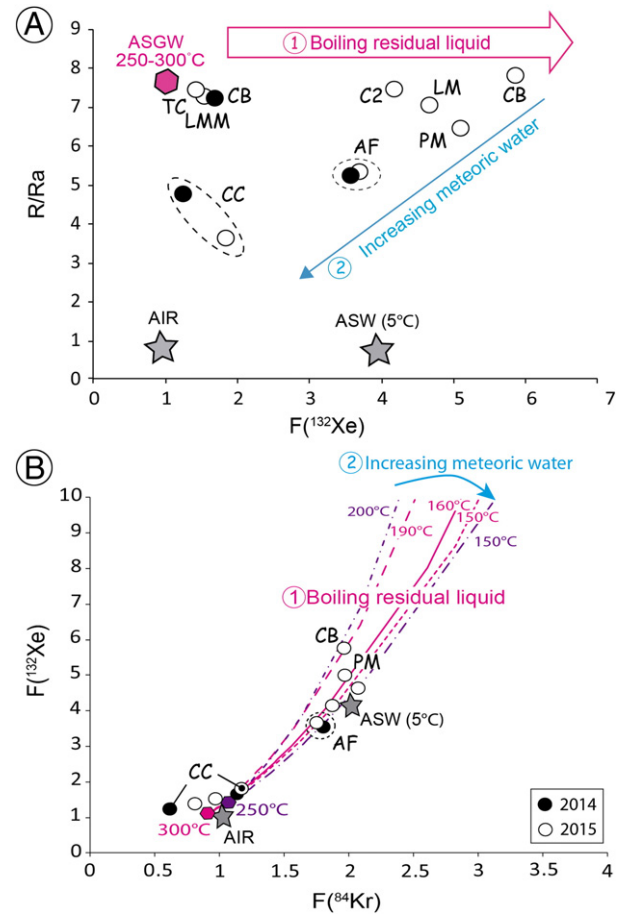

Fig. 4. A) $F(^{132}Xe)$ ratios plotted against R/Ra ratios. The isotopic variations of helium and elemental abundance of atmospheric noble gases can be explained by boiling and steam separation followed by massive ASW recharge. ASGW is for Air-Saturated Geothermal Water and represents the initial noble gas composition of deep CCVC reservoir. ASW: Air-Saturated Water at 5 °C (estimated for CCVC system). B) $F(^{132}Xe)$ vs. $F(^{84}Kr)$ ratios. (1) The pink curves are simulated considering an initial ASGW of 300 °C followed by boiling and steam separation at lower temperatures of 190 °C, 160 °C and 150 °C (Rayleigh distillation) due to water injection. (2) The purple curves are simulated considering an initial ASGW of 250 °C followed by boiling and steam separation at lower temperatures of 200 °C and 150 °C (Rayleigh distillation) due to water injection. For the Rayleigh distillation, it is assumed that the vapor phase is continuously removed from the system (Ma, 2009). Solubility values from Crovetto et al. (1982) and Ozima and Podosek (2002). $F(X) = (X / ^{36}Ar)_{sample} / (X / ^{36}Ar)_{Air}$. PM: Pucon-Mahuida; TC: Termas Copahue; AF: Anfiteatro; CC: Chanco-co; LM: Las Maquinas; LMM: Las Maquinitas; CB: Cabañita; C2: COP-2.

the atmosphere (Air), Air-Saturated Water (ASW) at 5 °C, and Air-Saturated Geothermal Water (ASGW) at a reservoir temperature of 250–300 °C (CO$_2$-CH$_4$ production; Agusto et al., 2013) are also reported

Table 3
Gas elemental composition of the CCVC geothermal fluids.

Sample	Field zone	Type	^4He (cm^{3}STP/cm^3) ×10^{-5}	^{20}Ne (cm^{3}STP/cm^3) ×10^{-8}	^{36}Ar (cm^{3}STP/cm^3) ×10^{-7}	^{84}Kr (cm^{3}STP/cm^3) ×10^{-9}	^{132}Xe (cm^{3}STP/cm^3) ×10^{-10}	F (^{20}Ne)	F (^{132}Xe)	F (^{84}Kr)
COP-CC-FI-14	Chanco-co (CC)	Fumarole	0.57	1666.42	295.39	404.64	249.76	1.08	1.13	0.66
COP-AF-FI-14	Anfiteatro (AF)	Fumarole	4.95	85.03	43.75	162.85	116.20	0.37	3.56	1.80
COP-CB-FI-14	Cabañita (CB)	Fumarole	3.41	142.11	29.67	69.59	37.08	0.91	1.68	1.13
COP-CC2-FI-15	Chanco-co (CC)	Fumarole	1.79	1883.32	403.26	974.28	549.90	0.89	1.83	1.17
COP-AF-FI-15	Anfiteatro (AF)	Fumarole	5.00	70.43	38.67	139.86	106.20	0.35	3.68	1.75
COP-CB-FI-15	Cabañita (CB)	Fumarole	2.56	3.92	1.89	7.68	8.16	0.40	5.78	1.96
COP-LM-FI-15	Las Maquiñas (LM)	Fumarole	2.87	5.11	1.38	5.93	4.81	0.70	4.65	2.07
COP-LMM-BG-15	Las Maquiñitas (LMM)	Bubbling gas	3.58	290.53	84.11	165.94	95.98	0.66	1.53	0.95
COP-2-GW-15	COP-2 (C2)	Well	3.48	14.48	5.38	20.79	16.70	0.51	4.16	1.87
COP-TC-BG-15	Termas Copahue (TC)	Bubbling gas	3.78	223.40	83.10	141.17	87.62	0.51	1.41	0.82
COP-PM-BG-15	Pucon Mahuida (PM)	Bubbling gas	0.49	33.76	17.26	70.19	64.57	0.37	5.02	1.97

(Crovetto et al., 1982; Ozima and Podosek, 2002). Most of CCVC fluid samples display a constant R/Ra (~7.5Ra) with the increase of $F(^{132}Xe)$, departing from the expected ASGW composition. This could be explained by fractionation of noble gases due to boiling and steam separation. However, R/Ra and $F(^{132}Xe)$ for Pucon-Mahuida (PM), Anfiteatro (AF), and Chancho-co (CC) gradually decrease from the Cabañita (CB) values. This, in conjunction with what was previously stated based on the He-N_2-Ar ternary diagram (Fig. 2) about these three locations (i.e. PM, AF, and CC show a mixing with ASW and/or air components), supports the conclusion that PM, AF, and CC may be the result of massive ASW and air addition from meteoric water probably related to the interaction with groundwater at shallow depth. Finally, this Fig. 4A indicates that samples 2015 LMM, 2015 TC and 2014 CB, plotted close to ASGW (geothermal compositional field), represent the initial isotopic composition of geothermal system.

Fig. 4B displays $F(^{132}Xe)$ versus $F(^{84}Kr)$ values in the CCVC fluids. Most samples start from ASGW elemental compositions and are explained by two processes: 1) boiling and steam separation at hydrothermal reservoir depth and 2) mixing with meteoric water and/or air (probably at shallow depth). During boiling and steam separation, more soluble heavier noble gases (Kr and Xe compared to Ar) are retained in the residual liquid. This process of elemental fractionation can be modeled as a Rayleigh distillation process, if we assume that the vapor phase is continuously removed from the system. In residual liquid, this process is given by the following equation (Ma, 2009):

$$(i/^{36}Ar)_w = (i/^{36}Ar)_{ASGW} \times f\left(k^i{}_w/k^{Ar}{}_w - 1\right) \qquad (2)$$

where $f^{36}Ar$ is the fraction of ^{36}Ar remaining in the residual liquid following boiling and steam separation and k is the solubility value (Crovetto et al., 1982; Ozima and Podosek, 2002).

In Fig. 4B, the pink and purple curves are simulated considering an initial ASGW of 250 (purple diamond) and 300 °C (pink diamond) followed by boiling and steam separation at lower temperature, from 200 °C to 150 °C. These simulations reproduce the elemental fractionation pattern observed in the CCVC fluids. Most $F(^{132}Xe)$ and $F(^{84}Kr)$ data for the CCVC fluids plot close to the simulated fractionation curves for a residual liquid after steam separation (Fig. 4B) or close to ASGW (pink and purple diamonds), with the exception of the CC sample collected in 2014 that plots at slightly lower $F(^{84}Kr)$. This 2014-CC sample can be explained by a second process of elemental fractionation compatible with a separated steam phase, as observed in Los Azufres fluids (Mexico; Pinti et al., 2013). Alternatively, this 2014-CC value may also reflect a strong level of atmospheric contamination as observed in Fig. 4A.

In summary, with the exception of 2015-TC, 2014-CB, and 2015-LMM, all samples show strong elemental fractionation of noble gases due to boiling and steam separation in the hydrothermal reservoir, providing fluids to the geothermal fields of CCVC. Anfiteatro (AF), located at the northwestern part of CCVC, and Chancho-co, located at the northern flank of Copahue are strongly contaminated by air related to the involvement of meteoric water probably from shallow aquifer (fluid-rock-water interaction). This is consistent with the hypothesis presented in Roulleau et al. (2015a) that Anfiteatro lies outside the high vapor zone which facilitates the direct ascent of hydrothermal fluids to the surface. Pucon-Mahuida (PM) is also significantly contaminated by air. This hydrothermal area is located in the southern flank of Copahue volcano and could be defined as a particular water recharge area as it was proposed that the flank of Copahue is a preferential zone for water recharge (Agusto et al., 2013; Velez et al., 2011).

5.2. δD-H₂O, δ¹⁸O-H₂O δ¹³C signature in CCVC fluids

The water isotopes could be investigated to determine the origin of the geothermal fluids and also to characterize chemical and physical processes such as water-rock interaction and boiling process (evaporation).
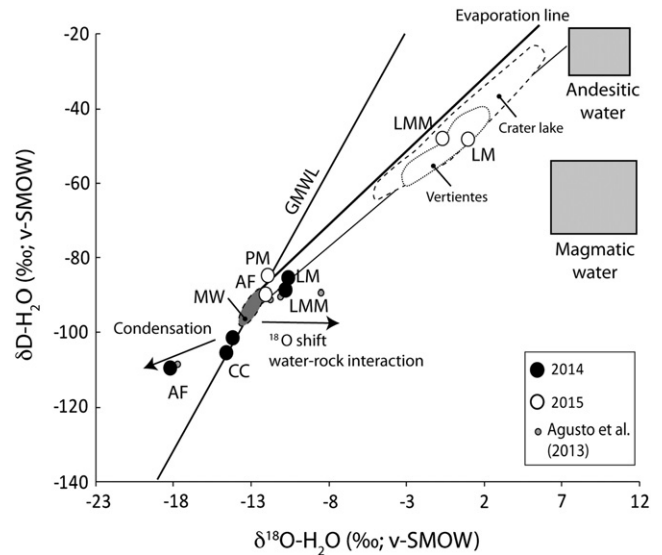

Fig. 5. Plot of δD-H_2O vs. $\delta^{18}O$-H_2O for the CCVC fluids collected in 2014 and 2015. The Global Meteoric Water Line (GMWL; Craig, 1961), andesitic water (Giggenbach, 1992) and magmatic water (Sheppard and Epstein, 1970) are reported. Vertientes and Crater lake data are from Agusto and Varekamp (2015). Evaporation line is defined from the calculation reported in Varekamp and Kreulen (2000). Andesitic water is defined as the isotopic composition of recycled seawater coming from the subduction zone. Magmatic water represents the isotopic composition of water in equilibrium with an unaltered magmatic body.

Fig. 5 presents the δD-H₂O versus δ¹⁸O-H₂O plot, where the Global Meteoric Water Line (GMWL; Craig, 1961), andesitic water field (Giggenbach, 1992), and magmatic water field (Sheppard and Epstein, 1970) are reported. Andesitic water is defined as the isotopic composition of recycled seawater coming from the subduction zone. Magmatic water represents the isotopic composition of water in equilibrium with an unaltered magmatic body. The H and O isotopic data from 2014 plot close to meteoric water (MW: Agusto et al., 2013) and on the GMW line, supported the meteoric water origin of CCVC fluids. Agusto et al. (2013) observed the same for condensate samples collected in 2012. The authors have suggested that the geothermal fluids were less enriched in ¹⁸O than the GMWL due to the water-rock interaction. This hypothesis may be consistent with the elemental noble gas data (Table 3) that show the evidence of the interaction of geothermal fluids with meteoric water (low $F(^{132}Xe)$) and host rocks (moderate R/Ra). Furthermore, the particular shift for AF sample could be explained by condensate process at shallow depth (Guleç, 2013). However, the isotopic trends of 2015-LMM and 2015-LM samples plot slightly towards the isotopic composition of andesitic waters. From the previous Section 5.1, 2015-LMM was characterized as a sample representative of the initial composition of the geothermal system whereas 2015-LM was defined as a sample affected by a boiling separation process at lower temperature (150 °C) than the geothermal temperature (250 °C–300 °C). These two samples have a similar composition as that of Copahue summit hot springs (called Vertientes; Vi) and Copahue crater lake (Agusto and Varekamp, 2015). Agusto and Varekamp (2015) published the values of δD-H₂O and δ¹⁸O-H₂O from Vertientes hot springs and Copahue crater lake that are presented in Fig. 5. The authors by the correlation between δ¹⁸O-H₂O and Cl⁻ (mg/L) showed that the Vertientes hot springs were a combination of meteoric and andesitic water whereas Copahue crater lake was the result of a combination of meteoric and andesitic water, and evaporation process (evaporation line was estimated from Varekamp and Kreulen, 2000). Thus, the Vertientes hot springs are representative of the volcano-hydrothermal composition. However, what is the origin of this shift on the δD-H₂O and δ¹⁸O-H₂O observed in samples LMM and LM collected in 2015? This change in δD-H₂O and in δ¹⁸O-H₂O between 2014 and 2015 for the samples LMM and LM may be the result of two

processes 1) magmatic contribution, consequently higher magmatic input in the CCVC geothermal system (consistent with the Vertiente composition) and 2) evaporation process as it is proposed for the water isotopic composition of Copahue crater lake. At this step, it is difficult to prove one or another hypothesis. To confirm one of these hypotheses, we compared the water and carbon isotope evolution between 2014 and 2015.

Fig. 6 presents $\delta^{13}C$-CO_2 values against $CO_2/^3He$ ratios from the CCVC fluids. Typical $CO_2/^3He$ and $\delta^{13}C$-CO_2 values for MORBs are 2×10^9 and $-6.5 \pm 2.5‰$, respectively (Sano and Marty, 1995; Sano and Williams, 1996). The $CO_2/^3He$ ratio for the crust ranges from 1×10^{12} to 1×10^{14}, whereas its $\delta^{13}C$–CO_2 composition varies between two major components (Hoefs, 2009): (1) organic sediments ($-40‰$ to $-20‰$), and (2) marine limestone (including slab carbonates) ($0 \pm 2‰$). For comparison, the volcanic arc average values for $CO_2/^3He$ and $\delta^{13}C$-CO_2 are $1.5 \pm 1.1 \times 10^{10}$ (Sano and Williams, 1996) and $-5.5 \pm 2.2‰$ (Sano and Marty, 1995), respectively.

The mixing curve follows:

$$\delta^{13}C_{obs} = Lim\ \delta^{13}C_{Lim.} + Morb\ \delta^{13}C_{MORB} + Sed\ \delta^{13}C_{Sed} \quad (3)$$

$$1/(CO_2/^3He)_{obs} = Lim/(CO_2/^3He_{Lim}) + Morb/(CO_2/^3He_{MORB}) + Sed/(CO_2/^3He_{Sed}) \quad (4)$$

$$MORB + Sed + Lim = 1 \quad (5)$$

where obs, Lim, Morb, and Sed refer to: the observed value, Limestone, MORB, and sediments, respectively.

The carbon contribution of the CCVC gases is as follows: 56–74% limestone, 16–34% organic sediments, and 2–30% MORB (Table 2). However, we note a significant difference of $CO_2/^3He$ and $\delta^{13}C$–CO_2 for samples collected in 2014 versus 2015. Our samples collected in 2014 present similar carbon compositions as for the samples collected in 2012 by Agusto et al. (2013). In contrast, our samples collected in 2015 display lower $CO_2/^3He$ and $\delta^{13}C$–CO_2 values compared to the ones for 2006–2007 and 2012 (Agusto et al., 2013), and 2014. The average $\delta^{13}C$–CO_2 and $CO_2/^3He$ compositions for the 2014 CCVC gas samples (excluding PM and CC samples that depart from the main cluster of points) are $-7.84‰$ and 12.1×10^9, respectively. The 2015 CCVC fluids average

changes to $-6.5‰$ and 6.4×10^9, respectively (excluding PM and CC). For the two field campaigns, LMM appears as the most primitive sample, with the lowest $\delta^{13}C$-CO_2 and $CO_2/^3He$: $-7.38‰$ and 5.5×10^9, respectively for 2014, and $-6.02‰$ and 4.67×10^9, respectively for 2015 (Fig. 6). The decrease of $CO_2/^3He$ and the increase of $\delta^{13}C$-CO_2 in our samples from 2014 to 2015 suggest a significant change in the chemistry of the CCVC fluids. The CC and PM samples present both the lowest $\delta^{13}C$-CO_2 values and the highest $CO_2/^3He$ ratios. This is an evidence for significant contamination by local sediments (organic sediments; Fig. 6).

There are two possible explanations for the observed isotopic and chemical variations: (1) a change in the sources and (2) a modification in the path for gas ascent. The gas compositions presented in this study reveal an increase trend between 2014 and 2015, mainly in the S_{total}, HCl and He contents (Table 1). However, no significant increase of Rc/Ra is observed, hence no new magmatic signature is detected. Furthermore, these changes are also associated with a combined increase of $\delta^{13}C$-CH_4 (from $-34.4‰$ for 2014 to $-28.07‰$ for 2015, LM sample, Table 2), δD-H_2O and $\delta^{18}O$-H_2O, suggesting a decrease of (meteoric) water-rock interaction in the hydrothermal system and a probable increase of the magmatic input. The same compositional and isotopic evolution is observed at Tatun volcano, Taiwan (Lan et al., 2007; Roulleau et al., 2015b). Based on unmodified He isotopic ratios, Lan et al. (2007) proposed that the carbon isotopic variation is the result of a modification in the path of gas ascent. Roulleau et al. (2015a) proposed that the variation of carbon composition over time is the result of variable amount of sediments versus limestone incorporation in the subduction zone, and/or variation of crustal contamination from local sediments. Thus, it is reasonable to argue for a higher magmatic input related to the modification of the gas ascent path that may generate in turn a decrease of local sediments contamination. This hypothesis needs to be confirmed through further monitoring in the field.

5.3. Origin of He and N in the CCVC fluids: interplay between MORB and sediments

The potential gas source of the CCVC fluids can be investigated by using N_2/He against $\delta^{15}N$ (Fig. 7; Fischer et al., 2002), where the nitrogen composition is represented by a mixing line between three
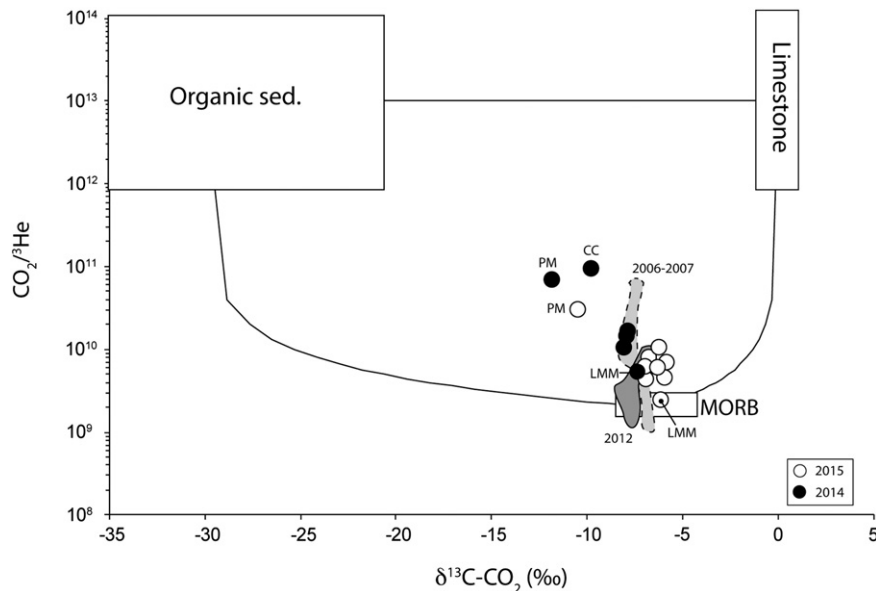

Fig. 6. $CO_2/^3He$ ratio versus $\delta^{13}C$–CO_2 values for the CCVC samples, compared to the MORB, organic sediments and marine limestone end-members. The solid lines represent mantle-organic sediments, mantle-marine limestone, and organic sediment-marine limestone binary mixing lines. MORB has $\delta^{13}C$–$CO_2 = -6.5 \pm 2.2‰$ and $CO_2/^3He = 2 \times 10^9$ (Marty et al., 1989; Sano and Marty, 1995; Sano and Williams, 1996). The $\delta^{13}C$–CO_2 and $CO_2/^3He$ values for organic sediments are $-30 \pm 10‰$ and 1×10^{13}, and $0 \pm 2‰$ and 1×10^{13} for marine limestone (Hoefs, 2009; Sano and Marty, 1995). Samples collected in 2006–2007 and 2012 are also reported for comparison (Agusto et al., 2013).
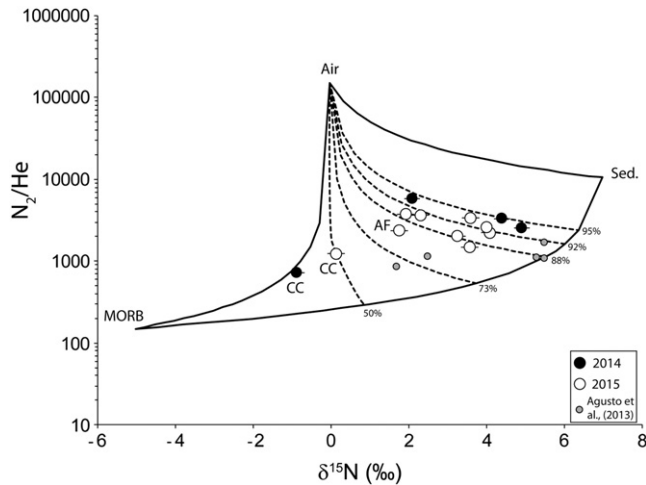
Fig. 7. Plot of N_2/He vs. $\delta^{15}N$, where the nitrogen composition is defined as a mixing line between three components (Marty and Zimmermann, 1999; Ozima and Podosek, 2002; Sano et al., 2001): air (0‰; 1.489×10^5), sediments ($+7 \pm 4$‰; 1.05×10^4), and MORB (-5‰; 150). Data from Agusto et al. (2013) are reported for comparison.

Fig. 8. Plot of Rc/Ra vs. $\delta^{15}N_c$ (‰) for the CCVC fluids. Air-corrected $\delta^{15}N$ values ($\delta^{15}N_c$) are calculated from the plot N_2/He vs. $\delta^{15}N$, as proposed by Fischer et al. (2002). Rc/Ra represents the air-corrected R/Ra. The three curves illustrate a mixing between a MORB-like mantle (variable He isotopic compositions) and subducted sediments ($+7$‰; Fischer et al., 2002; Sano et al., 2001). The air-corrected $\delta^{15}N$ values can be calculated using the equation: $\delta^{15}N_C = f \times \delta^{15}N_{MORB} + (1 - f) \, \delta^{15}N_{Sed}$ where $\delta^{15}N_{MORB} = -5$ ‰, $\delta^{15}N_{Sed.} = +7$‰, and f is the fraction of mantle-derived nitrogen (calculated as: $f = 1 - (\%\text{sed.}/100)$). Only samples with high Rc/Ra have been plotted that represent the original magmatic source from CCVC unlike to moderate Rc/Ra samples (CC, AF and PM) that show fluid-rock interaction in the shallow system.

components (Marty and Zimmermann, 1999; Ozima and Podosek, 2002; Sano et al., 2001): air ($\delta^{15}N = 0$‰; N_2/He $= 1.489 \times 10^5$), sediments ($+7 \pm 4$‰; 1.05×10^4), and MORB (-5‰; 150).

The mixing curve follows:

$$\delta^{15}N_{obs} = \text{Air } \delta^{15}N_{Air} + \text{Morb } \delta^{15}N_{Morb} + \text{Sed } \delta^{15}N_{Sed} \quad (6)$$

$$1/(N_2/He)_{obs} = \text{Air}/(N_2/He_{Air}) + \text{Morb}/(N_2/He_{Morb}) \\ + \text{Sed}/(N_2/He_{Sed}) \quad (7)$$

$$\text{Morb} + \text{Sed} + \text{Air} = 1 \quad (8)$$

where obs, Air, Morb, and Sed refer to: the observed value, Air, Morb, and sediments, respectively. All calculations are presented in Table 2.

The CCVC fluids (from Las Maquinas, Las Maquinitas, Termas de Copahue, and COP-2) have $\delta^{15}N$ values that are mostly higher than air (1.95‰ to 4.93‰), and a N_2/He ratio falling between 1795 and 3822 (Fig. 7), consistent with the published range for arc-related volcanoes (de Moor et al., 2013a; Fischer et al., 2002; Roulleau et al., 2013, 2015b; Sano et al., 2001). Chancho-co and Anfiteatro gases show lower $\delta^{15}N$ values (-1.46‰ to 2.11‰) and variable N_2/He, consistent with the incorporation of air and/or fluid-rock interaction in shallow system. This is also supported by their lowest R/Ra ratios.

The addition of sediment-derived nitrogen to the mantle source is expected to result in higher N_2/He ratios and $\delta^{15}N$ values. This tendency is observed for our CCVC samples (Fig. 7). Assuming that nitrogen and helium are not fractionated by magmatic or hydrothermal processes, we can estimate the proportion of nitrogen derived from sediments and a MORB-type mantle (Table 2). Using the percentage of sediments estimated for each sample we calculate the air-corrected $\delta^{15}N$ values ($\delta^{15}N_c$) based on the following equation:

$$\delta^{15}N_C = f \times \delta^{15}N_{MORB} + (1 - f) \, \delta^{15}N_{Sed.} \quad (9)$$

where $\delta^{15}N_{MORB} = -5$‰, $\delta^{15}N_{Sed.} = +7$‰, and f is the fraction of mantle-derived nitrogen (calculated as: $f = 1 - (\%\text{sed.}/100)$) (Table 2).

Fig. 8 presents the air-corrected ^{3}He/^{4}He ratios (Rc/Ra) versus the air-corrected $\delta^{15}N$ ($\delta^{15}N_c$) values excluding samples from CC and AF that appear to not represent the original magmatic source (see previous section). The binary mixing between MORB and sediments (from the slab) allows us to determine the pristine isotopic composition of helium and nitrogen: 7.7Ra and $+6$‰, respectively. Our mixing models suggest
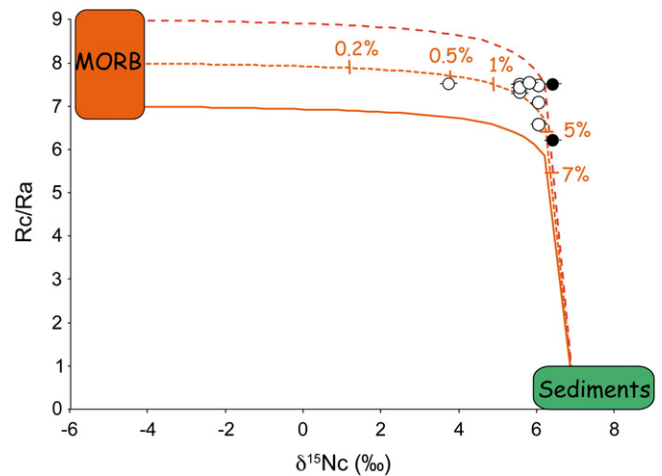
the involvement of 0.5% to 5% of subducted sediments in the CCVC magmatic source (Table 2).

5.4. Sulfur isotopes: predominance of a MORB-type signature

Hydrothermal gases are characterized by the virtual absence of SO_2 and the presence of H2S as unique S-bearing gaseous species (Giggenbach, 1980). Therefore, the isotopic composition of H2S can be very important for establishing the origin of S.

MORBs have a $\delta^{34}S$ of $+0.3 \pm 0.5$‰ (Sakai et al., 1984) with S/^{3}He ratio of $4.2 \pm 1.2 \times 10^7$ (Kagoshima et al., 2015). Modern sediments show a large range of $\delta^{34}S$ values, from -50‰ to $+21$‰ (Stefánsson et al., 2015 and reference therein; Thode, 1991), while water from rain and snow lies at $+2$‰ to $+9$‰ (Thode, 1991). The $\delta^{34}S$ values of arc lavas have been attributed to the recycling of subducted sulfate through subduction zones (Giggenbach, 1992; González-Partida et al., 2005; Matsuda et al., 2005; Stefánsson et al., 2015), while those of high temperature volcanic gases in global arc systems are due to mixing of subducted sulfate and sedimentary pyrite (Kagoshima et al., 2015). Sulfur isotopic fractionation is common in magmatic and hydrothermal systems (de Moor et al., 2013b; González-Partida et al., 2005; Marini et al., 2011; Matsuda et al., 2005; Stefánsson et al., 2015) and is controlled by various parameters such as the sulfur valence state (gas/melt and vapor/fluid/solid), the crystallization of S-bearing minerals, the degassing process, and the temperature (Marini et al., 2011).

The sulfur isotope compositions are investigated in the CCVC fluids (Fig. 9) ranging from -4.86‰ (TC) to $+2.77$‰ (LM) and an average of -1.58‰, lighter than those of high temperature volcanic gases with the average of $+4.6$‰. As similarly observed for geothermal/hydrothermal systems in Japan and Mexico (González-Partida et al., 2005; Matsuda et al., 2005), the CCVC gases have a large range of $\delta^{34}S$ values, suggesting that the sulfur source composition has been modified in the hydrothermal or magmatic system.

Boiling can have significant effects on the sulfur isotopic composition and S/^{3}He ratio in geothermal system. The isotopic compositions of sulfur in over 105 samples of pyrite from five deep wells of the Los Humeros geothermal field, Mexico, were determined by Martinez Serrano et al. (1996) along with the $\delta^{34}S$ values of dissolved sulfide and sulfate. The $\delta^{34}S$ values of pyrite and H2S are similar and vary between
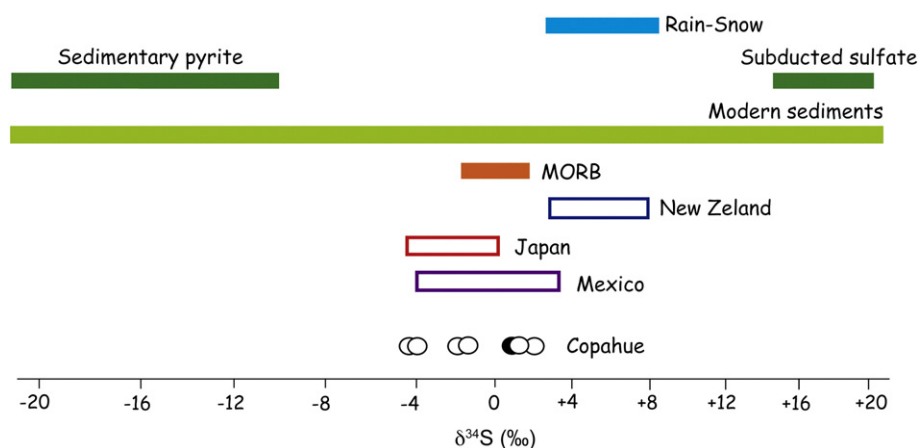
Fig. 9. $\delta^{34}S$ of the CCVC fluids compared to other volcanic arc data and the MORB end-member (Giggenbach, 1992; González-Partida et al., 2005; Matsuda et al., 2005; Stefansson et al., 2015). Modern sediment and Rain-Snow data from Marini et al. (2011) and Thode (1991). Subducted sulfate and Sedimentary pyrite are defined by Kagoshima et al. (2015).

−4.5 and +4.5‰, around an average of +0.02‰, suggesting that the provenance of sulfur involves a magmatic source. However, the $\delta^{34}S$ values of pyrite from four wells, with an average of −0.4‰, are slightly more negative than those from the fifth borehole, with a mean of +2‰. The largest changes in the isotopic characteristics of pyrite and H_2S were observed at depths where boiling and mixing phenomena occur. Another study from González-Partida et al. (2005) reported the isotopic compositions of hydrothermal pyrite in the Los Azufres geothermal field, Mexico. Two different groups were identified: (1) the pyrite samples coming from deep zones, where boiling does not occur, with $\delta^{34}S$ values of −1.6 to −3.0‰; and (2) the pyrites sampled from steam-dominated at shallow levels, with $\delta^{34}S$ values of −4 to −4.8‰. The average $\delta^{34}S$ value of pyrite, −2.5‰, is similar to that of H_2S, −2.0‰. The authors suggested that: (1) the initial isotopic value for sulfur in the geothermal reservoir, −2.3‰, implies a magmatic source; and (2) the values strongly depleted in ^{34}S observed in pyrites from shallow levels are produced by fractionation during boiling of hydrothermal fluids.

Considering the large range of $\delta^{34}S$ values observed in Copahue geothermal fluids (−4.86‰ to +2.77‰) and the conclusions of these two previous studies, we could argue for the sulfur fractionation by boiling process in the geothermal reservoir from Copahue. Another argument for this conclusion is the particular large change in sulfur composition from vent to vent that suggests that the effects of shallow processes on the $\delta^{34}S$ value of H_2S are important. In this condition, it is difficult to access the magmatic composition of Copahue geothermal fluids. Previous authors (Agusto et al., 2013; Varekamp et al., 2009) have been suggested that the well COP-2 has a composition representative of the magmatic-hydrothermal system. In this way, the sulfur composition of Copahue magmatic system will be −2.38‰, however, this sample seems to be also affected by part of boiling separation process as it was showed with elemental noble gas previously. In the future, the $\delta^{34}S$ value of total sulfur could be coupled together with $S/^3He$ ratio to provide another information as it was proposed by Kagoshima et al. (2015).

5.5. Isotopic composition of the CCVC fluids versus tectonic features

In the Andean SVZ, geothermal activity occurs in close spatial relationships with active volcanism along the Cordillera, which is primarily controlled by the ~1000 km long, NNE-trending Liquiñe-Ofqui Fault Zone (LOFZ), an intra-arc dextral strike-slip fault system associated with second-order anisotropy of overall NE-SW (extensional) and NW-SE (compressional) orientation (Fig. 1) (Cembrano et al., 1992, 1996, 2000; Cembrano and Lara, 2009). Rosenau et al. (2006) proposed that the particular location of CCVC is the result of the NE-striking extensional and transtensional faults that form an accommodation zone arrangement with a horse tail-like geometry; in brittle terminations, the

displacement is distributed through several branching splay faults. These small faults, curved away from the strike of the main fault, form an open imbricate fan. These structures, due to their high permeability, promote the formation of vertical fluid pathways (Rowland and Simmons, 2012) in favor of geothermal and hydrothermal system appearance.

Fig. 10 illustrates the fluid circulation and the water-rock interaction observed in the geothermal system of CCVC. The $^3He/^4He$ (7.7Ra), $\delta^{15}Nc$ (+6‰), and $\delta^{13}C$ (−6.5‰) for Las Maquinas, Las Maquinitas, Cabañita, and Termas Copahue are the most primitive values measured in the Chilean Andes (Hilton et al., 1993; Ray et al., 2009; Tardani et al., 2016), and are in the range of those measured in subduction zones (Hilton et al., 2002). These geothermal areas are directly associated with a NE fault network (Chiodini et al., 2015; Roulleau et al., 2016) defined as a group of new faults associated with the volcanic activity of Copahue volcano (JICA, 1992). These NE faults are directly connected to a high vapor zone located at a depth of ~200 m, which represents a preferential area for hydrothermal fluid ascent (Roulleau et al., 2016).

The moderate Rc/Ra (5.4Ra) and $\delta^{15}Nc$ (+1.9‰) for Anfiteatro, associated with a low δD-H_2O and $\delta^{18}O$-H_2O, clearly indicate that the magmatic source was diluted by addition of radiogenic He from meteoric water and local organic sediments (water-rock interaction). The dilution of magmatic fluids is favored by preferential infiltration of meteoric water through the low permeability of WNW faults (JICA, 1992). The meteoric water goes through the shallow depth of these faults down to the water table where there are formed ponds (Roulleau et al., 2015a, 2016). A small contribution of such fluids circulates from the NE fault that connects the high vapor zone to Anfiteatro. This contribution is weak because Anfiteatro is located outside the high vapor zone at the NW limit (Roulleau et al., 2016; Chiodini et al., 2015).

Pucon Mahuida and Chancho-co are located on the southern and northern flanks of Copahue volcano, respectively. They are direct manifestations of the magmatic-hydrothermal system of the volcano (Agusto et al., 2013; Panarello, 2002).

Fluids from Pucon Mahuida have high Rc/Ra (~6.4Ra), low $\delta^{13}C$-CO_2 (−11.1‰), and high $\delta^{15}Nc$ (~4.2‰), consistent with a mixing between volcanic fluids (magmatic-hydrothermal) and local organic sediments. This is consistent with the inferred NE fault network that has been reported by Rojas Vera et al. (2009).

The Chancho-co fluids are characterized by moderate Rc/Ra (4.18Ra to 5.19Ra) and low $\delta^{15}Nc$ (~−1.1‰), $\delta^{13}C$-CO_2 (~−9.0‰), δD-H_2O, and $\delta^{18}O$-H_2O. They also have high H_2S (S_{total} as H_2S only) and H_2, along with low CO_2 contents (Table 1). All these geochemical features suggest important dilution of the magmatic source by meteoric water and contamination by local organic sediments during water-rock interaction. This is consistent with the location of Chancho-co along a major
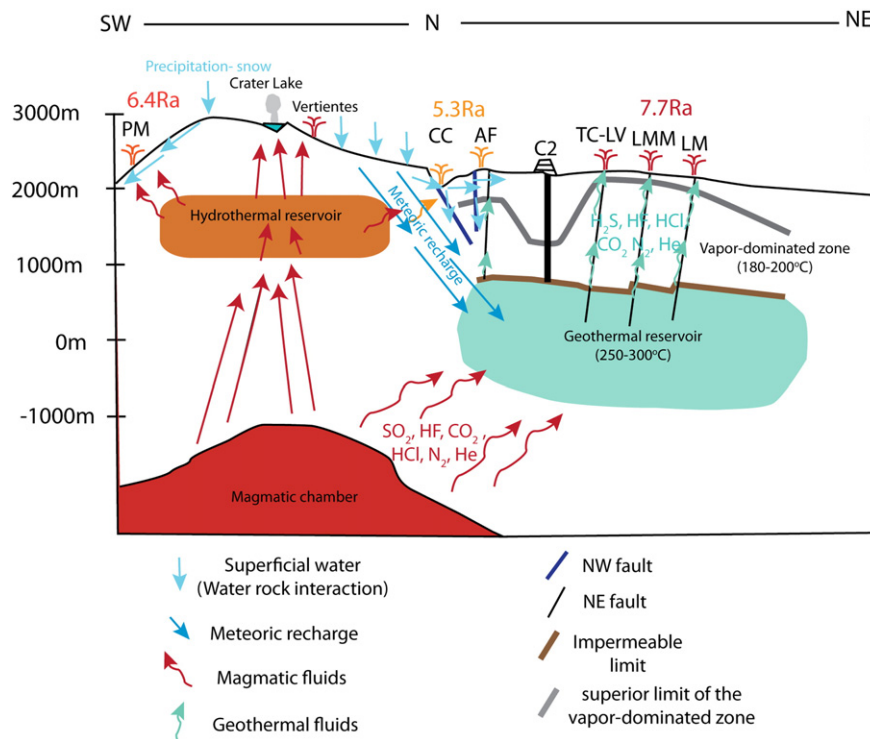
Fig. 10. Schematic model of fluid circulation from the geothermal system of CCVC. This model was performed using the compilation of data from Agusto et al. (2013), Velez et al. (2011), Roulleau et al. (2016), Rojas Vera et al. (2009), JICA (1992) and data from this study. This model suggests the direct ascent of the geothermal fluids at TC-LV, LMM and LM through the NE faults that are characterized by a high permeability. This is illustrated by high R/Ra observed in these areas. CC and AF, at the west limit of the geothermal reservoir, are located along WNW faults that are a preferential channel for water down flow and consequently water-rock-fluid interaction at shallow depth. This is illustrated by low to moderate R/Ra in these two areas.

WNW fault considered inefficient for hydrothermal fluid ascent but efficient for meteoric water infiltration (Roulleau et al., 2015a, 2016). H_2S is directly linked to the volcanic activity; it is commonly observed in volcanic and geothermal areas. However, the high H_2S contents of Chancho-co samples cannot be only related to its volcanic origin. H_2S is also formed by the decomposition of organic material by bacteria. This process is inferred to be part of the H_2S source for the Chancho-co fluids and should be verified by $S_{total}/^3He$ in the future.

In summary, we provide insights here that the CCVC structures control the geochemical and isotopic features of the fluids and hence, the whole geothermal system. Of particular importance are the NE faults that are thought to be direct pathways for fluid circulation from the magmatic source up to the surface.

6. Conclusions

We measured noble gas (He, Ne, Ar, Kr, and Xe) and stable (δD, $\delta^{13}C$, $\delta^{15}N$, $\delta^{18}O$, and $\delta^{34}S$) isotopes in several geothermal and hydrothermal samples from the CCVC. The goal of this work was to provide insights into the fluid circulation and evolution of this hydrothermal/geothermal system as controlled by the activity of Copahue volcano and the local structures. With the exception of Anfiteatro (up to 5.39Ra), the northeastern geothermal fields, composed of Las Maquinas, Las Maquinitas, Termas de Copahue, and Cabañita, provide the highest Rc/Ra in the studied area and in the entire SVZ (up to 7.86Ra in 2015). The hydrothermal activity observed at Pucon Mahuida (southern flank of Copahue volcano) and Chancho-co (northern flank of the volcano) exhibits moderate to low $^3He/^4He$ (up to 6.59Ra and up to 5.19Ra, respectively). The high elemental ratios of Xe and Kr observed for most CCVC gas samples are explained by elemental fractionation during boiling and steam separation at hydrothermal temperatures (250–300 °C). Rayleigh distillation curves simulate the CCVC fluid evolution, considering an initial ASGW of 250 °C and a temperature of 300 °C followed by boiling and steam

separation at lower temperature, from 200 °C to 150 °C. The low $^3He/^4He$ ratios are largely explained by meteoric water and air contamination, which follow the boiling-steam separation event. The hydrogen and oxygen isotopes present an increase from meteoric water to andesitic water signature between 2014 and 2015. This evolution is also associated with an increase of $\delta^{13}C$ values and S_{total}, HCl, and He contents, along with a decrease of $CO_2/^3He$ inferred to be the result of a change in the path of gas uprising, in turn inducing higher magmatic-hydrothermal contribution in the fluid signature. The composition of the magmatic source of the CCVC fluids is: $^3He/^4He = 7.7Ra$, $\delta^{15}N = +6‰$, and $\delta^{13}C = -6.5‰$. Mixing models between air-corrected He and N suggest the involvement of 0.5% to 5% of subducted sediments in the CCVC magmatic source. The magmatic sulfur isotopic composition is estimated at $-2.38‰$ (from COP-2), but most samples show elemental fractionation due to boiling and steam separation. The geochemical and isotopic features of the CCVC fluids illustrate the particular structural setting observed in this volcanic and geothermal area. NE faults promote the ascent of hydrothermal fluids in the geothermal area whereas WNW faults serve as preferential channels for meteoric water infiltration.

Appendix A

Table A1
Ne, Kr, Ar and Xe isotopic ratios.

Sample	Field zone	Type	$^{20}Ne/^{22}Ne$	+/-	$^{21}Ne/^{22}Ne$	+/-	$^{38}Ar/^{36}Ar$	+/-	$^{40}Ar/^{36}Ar$	+/-	$^{80}Kr/^{84}Kr$	+/-	$^{82}Kr/^{84}Kr$	+/-	$^{83}Kr/^{84}Kr$
Air			**9.8**		**0.029**		**0.188**		**295.5**		**0.039599**		**0.20217**		**0.20136**
COP-CC-FI - 14	Chanco-co	Fumarole	9.5786	0.0170	0.0285	0.0001	0.1879	0.0002	294.7	0.1	0.0620	0.0002	0.2001	0.0002	0.1992
COP-AF-FI - 14	Anfiteatro	Fumarole	9.8716	0.0228	0.0292	0.0001	0.1881	0.0002	300.4	0.1	0.0369	0.0001	0.2026	0.0003	0.2015
COP-CB-FI- 14	Cabañita	Fumarole	9.9016	0.0221	0.0292	0.0001	0.1882	0.0003	301.1	0.2	0.0371	0.0001	0.2026	0.0001	0.2018
COP-LM-FI-15	Las Maquiñas	Fumarole	9.5427	0.0243	0.0269	0.0017	0.1850	0.0142	391.6	6.5	0.0360	0.0010	0.2022	0.0013	0.2021
COP-CB-FI -15	Cabañita	Fumarole	9.9256	0.0241	0.0295	0.0007	0.1858	0.0018	371.2	0.8	0.0359	0.0002	0.2036	0.0006	0.2027
COP-AF-FI -15	Anfiteatro	Fumarole	9.7683	0.0183	0.0290	0.0001	0.1882	0.0001	302.0	0.1	0.0368	0.0002	0.2022	0.0009	0.2014
COP-LMM-BG-15	Las Maquiñitas	Bubbling gas	9.7769	0.0037	0.0290	0.0000	0.1880	0.0001	298.1	0.1	0.0400	0.0001	0.2018	0.0004	0.2012
COP-2-GW-1 5	COP-2	Well	10.2231	0.0133	0.0299	0.0005	0.1850	0.0022	316.5	0.8	0.0359	0.0001	0.2032	0.0004	0.2023
COP-TC-BG-1 5	Termas Copahue	Bubbling gas	9.7680	0.0169	0.0290	0.0001	0.1880	0.0002	300.0	0.1	0.0394	0.0001	0.2029	0.0005	0.2013
COP-PM-15	Pucon Mahuida	Bubbling gas	9.8444	0.0037	0.0289	0.0001	0.1881	0.0003	299.1	0.1	0.0360	0.0001	0.2027	0.0004	0.2016
COP-CC2-FI- 15	Chanco-co	Fumarole	9.8618	0.0095	0.0292	0.0000	0.1881	0.0002	295.4	0.1	0.0408	0.0001	0.2027	0.0003	0.2015

Table A1 *(continued)*
Ne, Kr, Ar and Xe isotopic ratios.

+/-	$^{86}Kr/^{84}Kr$	+/-	$^{128}Xe/^{130}Xe$	+/-	$^{129}Xe/^{130}Xe$	+/-	$^{131}Xe/^{130}Xe$	+/-	$^{132}Xe/^{130}Xe$	+/-	$^{134}Xe/^{130}Xe$	+/-	$^{136}Xe/^{130}Xe$	+/-
	0.30524		**0.4715**		**6.496**		**5.213**		**6.607**		**2.563**		**2.176**	
0.0002	0.3033	0.0002	0.4784	0.0121	6.520	0.020	5.218	0.015	6.610	0.020	2.566	0.01	2.177	0.007
0.0003	0.3049	0.0004	0.4622	0.0100	6.504	0.027	5.217	0.022	6.606	0.029	2.556	0.01	2.172	0.010
0.0001	0.3052	0.0002	0.4882	0.0110	6.489	0.021	5.207	0.016	6.576	0.021	2.558	0.01	2.173	0.007
0.0016	0.3064	0.0015	0.5928	0.0305	6.294	0.091	5.066	0.074	6.439	0.092	2.466	0.04	2.117	0.036
0.0006	0.3065	0.0009	0.4857	0.0180	6.499	0.032	5.212	0.026	6.628	0.035	2.557	0.01	2.176	0.012
0.0009	0.3046	0.0013	0.4993	0.0119	6.507	0.030	5.218	0.024	6.614	0.031	2.559	0.01	2.175	0.011
0.0004	0.3049	0.0005	0.4394	0.0091	6.495	0.022	5.227	0.018	6.614	0.024	2.563	0.01	2.175	0.008
0.0004	0.3050	0.0006	0.4655	0.0139	6.520	0.031	5.241	0.025	6.617	0.032	2.554	0.01	2.163	0.010
0.0004	0.3055	0.0007	0.4768	0.0120	6.485	0.023	5.203	0.018	6.608	0.024	2.553	0.01	2.168	0.008
0.0004	0.3055	0.0007	0.4522	0.0101	6.510	0.027	5.221	0.022	6.637	0.029	2.572	0.01	2.180	0.010
0.0003	0.3052	0.0004	0.5454	0.0174	6.523	0.023	5.235	0.018	6.621	0.025	2.565	0.01	2.171	0.008

References

Agusto, M., 2011. Estudio geoquímico de los fluidos volcánicos e hidrotermales del Complejo Volcánico Copahue Caviahue y su aplicación para tareas de seguimiento (Ph.D.Thesis, 270 pp.).

Agusto, M., Varekamp, J., 2015. The Copahue Volcanic-Hydrothermal System and Applications for Volcanic Surveillance. In: Tassi, F., Vaselli, O., Caselli, A. (Eds.), Copahue Volcano: The Smoking Mountain Between Argentina y Chile. Springer.

Agusto, M., Tassi, F., Caselli, A., Vaselli, O., Tedesco, D., Poreda, R., 2007. Chemical and Isotopic Features of Thermal Fluid Discharges in the Volcano-Hydrothermal System of Caviahue-Copahue Volcanic Complex (Argentina). GEOSUR (International Geological Congress on the Southern Hemisphere), Santiago de Chile.

Agusto, M., Tassi, F., Caselli, A.T., Vaselli, O., Rouwet, D., Capaccioni, B., Caliro, S., Chiodini, G., Darrah, T., 2013. Gas geochemistry of the magmatic-hydrothermal fluid reservoir in the Copahue-Caviahue Volcanic Complex (Argentina). J. Volcanol. Geotherm. Res. 257, 44–56.

Caselli, A.T., Agusto, M.R., Fazio, A., 2005. Cambios térmicos y geoquímicos del lago cratérico del volcán Copahue (Neuquén): posibles variaciones cíclicas del sistema volcánico. Actas Del Congreso XVI Congreso Geológico Argentino 1, La Plata, pp. 332–336.

Caselli, A., Agusto, M., Velez, M.L., Forte, P., Bengoa, C., Daga, R., Albite, J.M., Capaccioni, B., 2015. The 2012 Eruption. In: Tassi, F., Vaselli, O., Caselli, A. (Eds.), Copahue Volcano: The Smoking Mountain Between Argentina y Chile. Springer International Publishing.

Cembrano, J., Lara, L., 2009. The link between volcanism and tectonics in the southern volcanic zone of the Chilean Andes: a review. Tectonophysics 471, 96–113.

Cembrano, J., Beck, M.E., Burmester, R.F., Rojas, C., Garcia, A., Herve, F., 1992. Paleomagnetism of Lower Cretaceous rocks from east of the Liquiñe-Ofqui fault zone, southern Chile: evidence of small in-situ clockwise rotations. Earth Planet. Sci. Lett. 113, 539–551.

Cembrano, J., Hervé, F., Lavenu, A., 1996. The Liquiñe-Ofqui fault zone: a long-lived intra-arc fault system in southern Chile. Tectonophysics 259, 55–66.

Cembrano, J., Schermer, E., Lavenu, A., Sanhueza, A., 2000. Contrasting nature of deformation along an intra-arc shear zone, the LOFZ fault zone, southern Chilean Andes. Tectonophysics 319, 129–149.

Chiodini, G., Cardellini, C., Lamberti, M.C., Agusto, M., Caselli, A., Liccioli, C., Tamburello, G., Tassi, F., Vaselli, O., Caliro, S., 2015. Carbon dioxide diffuse emission and thermal energy release from hydrothermal systems at Copahue-Caviahue Volcanic Complex (Argentina). J. Volcanol. Geotherm. Res. 304, 294–303.

Craig, H., 1961. Isotopic variations in meteoric waters. Science 133, 1702–1703.

Craig, H., Lupton, J.E., Horibe, Y., 1978. A mantle helium component in Circum-Pacific volcanic gases: Hakone, the Marianas, and Mr. Lassen. In: Alexander, E.C., Ozima, M. (Eds.), Advances in Earth and Planetary Science. (Terrestrial rare gases). Academic publication, Japan, pp. 3–16.

Crovetto, R., Fernandez-Prini, R., Japas, M.L., 1982. Solubilities of inert gases and methane in H_2O and in D_2O in the temperature range of 300 to 600 K. J. Chem. Phys. 76 (2), 1077–1086.

de Moor, J.M., Fischer, T.P., Sharp, Z.D., Hilton, D.R., Barry, P.H., Mangasini, F., Ramirez, C., 2013a. Gas chemistry and nitrogen isotope compositions of cold mantle gases from Rungwe Volcanic Province, southern Tanzania. Chem. Geol. 334, 30–42.

de Moor, J.M., Fischer, T.P., Sharp, Z.D., King, P.L., Wilke, M., Botcharnikov, R.E., Cottrell, E., Zelenski, M., Marty, B., Klimm, K., Rivard, C., Ayalew, D., Ramirez, C., Kelley, K.A., 2013b. Sulfur degassing at Erta Ale (Ethiopia) and Masaya (Nicaragua) volcanoes: implications for degassing processes and oxygen fugacities of basaltic systems. Geochem. Geophys. Geosyst. 14 (10), 4076–4108.

Fischer, T.P., Hilton, D.R., Zimmer, M.M., Shaw, A.M., Sharp, Z.D., Walker, J.A., 2002. Subduction and recycling of nitrogen along the Central American margin. Science 297, 1154–1157.

Giggenbach, W.F., 1975. A simple method for the collection and analysis of volcanic gas samples. Bull. Volcanol. 36, 132–145.

Giggenbach, W.F., 1980. Geothermal gas equilibria. Geochem. Cosmochem. Acta 44, 2021–2032.

Giggenbach, W.F., 1992. Isotopic shifts in waters from geothermal and volcanic systems along convergent plate boundaries and their origin. Earth Planet. Sci. Lett. 113 (4), 495–510.

Giggenbach, W.F., Goguel, R.L., 1989. Collection and analysis of geothermal and volcanic water and gas discharges. DSIR Chemistry, Report 2401.

Giggenbach, W.F., Poreda, R.J., 1993. Helium isotopic and chemical composition of gases from volcanic-hydrothermal systems in the Philippines. Geothermics 22, 369–380.

González-Partida, E., et al., 2005. Hydrogeochemical and isotopic fluid evolution of the Los Azufres geothermal field, Central Mexico. Appl. Geochem. 20, 23–39.

Guleç, N., 2013. Isotopes and gasgeochemistry of geothermal system. IGA Academy Reports 0112.

Hilton, D.R., Hammerschmidt, K., Teufel, S., Friedrichsen, H., 1993. Helium isotope characteristics of Andean geothermal fluids and lavas. Earth Planet. Sci. Lett. 120 (3–4), 265–282.

Hilton, D.R., Fischer, T.P., Marty, B., 2002. Noble gases and volatile recycling at subduction zones. In: Porcelli, D.P., Ballentine, C.J., Wieler, R. (Eds.), Reviews in Mineralogy and Geochemistry. Noble Gases in Geochemistry and Cosmochemistry, pp. 319–370.

Hoefs, J., 2009. Stable Isotope Geochemistry (288 pp.).

JICA, 1992. The Feasibility Study on the Northern Neuquen Geothermal Development Project. Japan International Cooperation Agency, Neuquen, p. 444.

Kagoshima, T., Sano, Y., Takahata, N., Maruoka, T., Fischer, T.P., Hattori, K., 2015. Sulfur geodynamic cycle. Sci. Rep. 5, 8330.

Kennedy, B.M., van Soest, M.C., 2006. A helium isotope perspective on the Dixie Valley, Nevada, hydrothermal system. Geothermics 35, 26–43.

Lan, T.F., Yang, T.F., Lee, H.F., Chen, Y.G., Chen, C.-H., Song, S.R., Tsao, S., 2007. Compositions and flux of soil gas in Liu-Huang-Ku hydrothermal area, northern Taiwan. J. Volcanol. Geotherm. Res. 165, 32–45.

Lee, H.F., Yang, T.F., Lan, T.F., Song, S.R., Tsao, S., 2005. Fumarolic gas composition of the Tatun Volcano Group, northern Taiwan. Terr. Atmos. Ocean. Sci. Techn. 16, 843–864.

Linares, E., Ostera, H.A., Mas, L., 1999. Cronología Potasio-Argón del complejo efusivo Copahue-Caviahue, Provincia de Neuquén. Rev. Asoc. Geol. Argent. 54 (3), 240–247.

Ma, L., 2009. Noble Gases Dissolved in Groundwaters of the Michigan Basin: Implications for Paleoclimatology, Hydrogeology, Tectonics and Mantle Geochemistry. (Doctor of Philosophy Thesis). University of Michigan (229 pp.).

Marini, L., Moretti, R., Accornero, M., 2011. Sulfur isotopes in magmatic-hydrothermal systems, melts, and magmas. Rev. Mineral. Geochem. 73 (1), 423–492.

Martinez Serrano, R., Jarcquier, B., Arnold, M., 1996. The $\delta^{34}S$ composition of sulfates and sulfides at the Los Humeros geothermal system, Mexico and their application to physicochemical fluid evolution. J. Volcanol. Geotherm. Res. 73 (1), 99–118.

Marty, B., 1984. On the noble gas isotopic fractionation in naturally occurring gases. Geochem. J. 18, 157–162.

Marty, B., Zimmermann, L., 1999. Volatiles (He, C, N, Ar) in mid-ocean ridge basalts: assessment of shallow-level fractionation and characterization of source composition. Geochim. Cosmochim. Acta 63 (21), 3619–3633.

Marty, B., Jambon, A., Sano, Y., 1989. Helium isotopes and CO_2 in volcanic gases of Japan. Chem. Geol. 76 (1–2), 25–40.

Mas, L.C., 2005. Present status of the Copahue geothermal project. World Geothermal Congress, Antalya, pp. 1–10.

Mas, L.C., Mas, G.R., 2015. Geothermal energy development at Copahue Volcano. In: Tassi, F., Vaselli, O., Caselli, A. (Eds.), Copahue Volcano: The Smoking Mountain Between Argentina y Chile. Springer.

Matsuda, K., Shimada, K., Kiyota, Y., 2005. Isotope techniques for clarifying origin of SO4 type acid geothermal-fluid. Case studies of geothermal areas in Kyushu, Japan. Use of Isotope Techniques to Trace the Origin of Acidic Fluids in Geothermal Systems, pp. 83–95.

Mazor, E., Truesdell, A.H., 1984. Dynamics of a geothermal field traced by noble gases: Cerro Prieto, Mexico. Geothermics 13 (1–2), 91–102.

Melnick, D., Folguera, A., Ramos, V.A., 2006. Structural control on arc volcanism: the Caviahue-Copahue complex, central to Patagonian Andes transition (38°S). J. S. Am. Earth Sci. 22 (1–2), 66–88.

Moreira, M., Kurz, D., 2013. Noble gases as tracers of mantle processes and magmatic degassing. In: Burnard, P. (Ed.), Advances in Isotopes GeochemistryThe Noble Gases as Geochemica Tracers. Springer-Verlag, Berlin Heidelberg, pp. 371–391.

Muñoz, J., Stern, C., 1988. The Quaternary volcanic belt of the southern continental margin of South America: transverse structural and petrochemical variations across the segment between 38° and 39°S. J. S. Am. Earth Sci. 1, 147–161.

Nakai, S., Wakita, H., Nuccio, M., Italiano, F., 1997. MORB-type neon in an enriched mantle beneath Etna, Sicily. Earth Planet. Sci. Lett. 153, 57–66.

Ozima, M., Podosek, F.A., 2002. Noble Gas Geochemistry. Cambridge University Press (300 pp.).

Panarello, H.O., 2002. Características isotópicas y termodinámicas de reservorio del campo geotérmico Copahue-Caviahue, provincia del Neuquén. Rev. Asoc. Geol. Argent. 57 (2), 182–194.

Pinti, D.L., Castro, M.C., Shouakar-Stash, O., Tremblay, A., Garduño, V.H., Hall, C.M., Hélie, J.F., Ghaleb, B., 2013. Evolution of the geothermal fluids at Los Azufres, Mexico, as traced by noble gas isotopes, $\delta^{18}O$, δD, $\delta^{13}C$ and $^{87}Sr/^{86}Sr$. J. Volcanol. Geotherm. Res. 249, 1–11.

Ray, M.C., Hilton, D.R., Munoz, J., Fischer, T.P., Shaw, A.M., 2009. The effects of volatile recycling, degassing and crustal contamination on the helium and carbon geochemistry of hydrothermal fluids from the Southern Volcanic Zone of Chile. Chem. Geol. 266 (1–2), 38–49.

Rojas Vera, E., et al., 2009. La neotectonica del arco volcanico a la latitud del volcan Copahue (38°S), Andes de Neuquen. Rev. Asoc. Geol. Argent. 65, 204–214.

Rosenau, M., Melnick, D., Echtler, H., 2006. Kinematic constraints on intra-arc shear and strain partitioning in the southern Andes between 38°S and 42°S latitude. Tectonics 25 (TC4013).

Roulleau, E., Sano, Y., Takahata, N., Kawagucci, S., Takahashi, H., 2013. He, N and C isotopes and fluxes in Aira Caldera: comparative study of hydrothermal activity in Sakurajima volcano and Wakamiko crater, Kyushu, Japan. J. Volcanol. Geotherm. Res. 258, 163–175.

Roulleau, E., Pizarro, M., Bravo, F., Muñoz, C., Sanchez, J., Esteban, C., de la Cal, F., 2015a. The Geothermal System of Copahue-Caviahue Volcanic Complex (Argentina): New Insights from Self-Potential, CO_2 and Temperature Measurements, With Structural and Fluid Circulation Implications. Congresso Geologico Chileno La Serena.

Roulleau, E., Sano, Y., Takahata, N., Yang, F.T., Takahashi, H.A., 2015b. He, Ar, N and C isotope compositions in Tatun Volcanic Group (TVG), Taiwan: evidence for an important contribution of pelagic carbonates in the magmatic source. J. Volcanol. Geotherm. Res. 303, 7–15.

Roulleau, E., Bravo, F., Barde-Cabusson, S., Pizarro, M., Muñoz, C., Sanchez, J., Tardani, D., Sano, Y., Takahata, N., de la Cal, F., Esteban, C., 2016. The Geothermal System of Caviahue-Copahue Volcanic Complex (Chile-Argentina): New Insights from Self-Potential, Soil CO_2 Degassing, Temperature Measurements and Helium Isotopes, With Structural and Fluid Circulation Implications. EGU, Viena, pp. 17–22 (April 2016).

Rowland, J.V., Simmons, S.F., 2012. Hydrologic, magmatic, and tectonic controls on hydrothermal flow, Taupo Volcanic Zone, New Zealand: implications for the formation of epithermal vein deposits. Econ. Geol. 107, 427–457.

Sakai, H., Marais, D.J.D., Ueda, A., Moore, J.G., 1984. Concentrations and isotope ratios of carbon, nitrogen, and sulfur in ocean-floor basalts. Geochim. Cosmochim. Acta 48, 2433–2441.

Sano, Y., Fischer, T., 2013. The analysis and interpretation of noble gases in modern hydrothermal systems. In: Burnard, P. (Ed.), The Noble Gases as Geochemical Tracers.

Sano, Y., Marty, B., 1995. Origin of carbon in fumarolic gas from island arcs. Chem. Geol. 119 (1–4), 265–274.

Sano, Y., Wakita, H., 1988. Helium isotope ratio and heat discharge rate in the Hokkaido Island, Northeast Japan. Geochem. J. 22, 293–303.

Sano, Y., Williams, S.N., 1996. Fluxes of mantle and subducted carbon along convergent plate boundaries. Geophys. Res. Lett. 23 (20), 2749–2752.

Sano, Y., Takahata, N., Nishio, Y., Fischer, T.P., Williams, S.N., 2001. Volcanic flux of nitrogen from the Earth. Chem. Geol. 171 (3–4), 263–271.

Sano, Y., Takahata, N., Seno, T., 2006. Geographical distribution of ^{3}He/^{4}He ratios in the Chugoku district, Southwestern Japan. Pure Appl. Geophys. 163, 745–757.

Sano, Y., Tokutake, T., Takahata, N., 2008. Accurate measurement of atmospheric helium isotopes. Anal. Sci. 24 (4), 521–525.

Sheppard, S.M.F., Epstein, S., 1970. D/H and ^{18}O/^{16}O ratios of minerals of possible mantle or lower crustal origin. Earth Planet. Sci. Lett. 9, 232–239.

Stefánsson, A., Keller, N.S., Robin, J.G., Ono, S., 2015. Multiple sulfur isotope systematics of Icelandic geothermal fluids and the source and reactions of sulfur in volcanic geothermal systems at divergent plate boundaries. Geochim. Cosmochim. Acta 165, 307–323.

Tardani, D., Reich, M., Roulleau, E., Takahata, N., Sano, Y., Perez-Flores, P., Sanchez, P., Cembrano, J., Arancibia, G., 2016. Exploring the feedbacks between structure and hydrothermal fluid composition using helium, nitrogen and carbon isotopes in a long-lived intra-arc strike slip fault. Geochim. Cosmochim. Acta 184, 193–211.

Tedesco, D., Nagao, K., Scarsi, P., 1998. Noble gas isotopic ratios from historical lavas and fumaroles at Mount Vesuvius (southern Italy): constraints for current and future volcanic activity. Earth Planet. Sci. Lett. 164 (1–2), 61–78.

Thode, H.G., 1991. Sulphur isotopes in nature and the environment: an overview. In: Grinenko, H.R.K.a.V.A. (Ed.), Stable Isotopes in the Assessment of Natural and Anthropogenic Sulphur in the Environment.

Trieloff, M., Kunz, J., Clague, D.A., Harrison, D., Allégre, C.J., 2000. The nature of pristine noble gases in mantle plumes. Science 288 (5468), 1036–1038.

Varekamp, J.C., Kreulen, 2000. The stable isotope geochemistry of volcanic lakes, with examples from Indonesia. JVGR 97, 309–327.

Varekamp, J.C., Ouimette, A.P., Herman, S.W., Bermédez, A., Delpino, D., 2001. Hydrothermal element fluxes from Copahue, Argentina: a beehive volcano in turmoil. Geology 29 (11), 1059–1062.

Varekamp, J.C., Ouimette, A.P., Herman, S.W., Flynn, K.S., Bermudez, A., Delpino, D., 2009. Naturally acid waters from Copahue volcano. Argentina. App. Geochem. 24, 208–220.

Varekamp, J.C., Ouimette, A.P., Herman, S.W., Flynn, K.S., Bermudez, A., Delpino, D., 2009. Naturally acid waters from Copahue volcano, Argentina. Appl. Geochem. 24 (2), 208–220.

Velez, M.L., Euillades, P., Caselli, A., Blanco, M., Diaz, J.M., 2011. Deformation of Copahue volcano: inversion of InSAR data using a genetic algorithm. J. Volcanol. Geotherm. Res. 202 (1–2), 117–126.